UNIVERSITÀ DEGLI STUDI DI NAPOLI

**“FEDERICO II”**

Facoltà di Scienze MM. FF. NN.

Corso di dottorato in DINAMICA INTERNA DI SISTEMI MAGMATICI

DI

VULCANI ATTIVI, XXI CICLO

***Ph.D thesis***

Rosario Esposito

# Geochemical study of the Solchiaro (Procida Island,Campi Flegrei) eruptive products by microthermometry and microanalyses of fluid and melt inclusions.

Tutors:

Prof. B. De Vivo (Università degli Studi di Napoli “Federico II”)

Prof. R. J. Bodnar (Virginia Polytechnic Institute and State University)

**Abstract**

This study presents the work I have done during the 4 years of a PhD program that was part of the internationalization programme of the Italian research system approved by the Ministero della Ricerca e dell'Università (MIUR) between the Università degli Studi di Napoli "Federico II", (Dipartimento di Scinze della Terra) and the Virginia Polytechnic Institute and State University (Department of Geosciences).

107 selected melt inclusion (MI), 77 open glasses, 80 olivines and 7 bulk rocks (from 4 representative samples of Solchiaro eruption) were analyzed for major/trace element and volatiles. Mostly, olivine compositions vary from $Fo_{82}$ to $Fo_{88}$ with one maximum value of $Fo_{90}$. 2 group of MI were recognized based on major element composition: 1) $K_2O$-rich MI with composition that is the same of bulk rock in the literature and 2) $K_2O$-poor MI that instead have been never reported from previous study of the Phlegrean Volcanic District (PVD). The first group consists of 95% of the melt and relates mostly to within plate setting whereas the second group consists of around 5% of the melt and relates to subduction setting. Magma associated with Solchiaro eruption evolved under open system processes as suggested by petrographic evidence and glass compositions. $H_2O$-$CO_2$ concentrations dissolved in glass suggest that magma was saturated in volatiles at least at 12.5 km depth and continuously degassed during the Solchiaro eruption. Maximum depths are in agreement with other studies based on different approaches. Volatile correlations suggest that during closed system degassing, as the Solchiaro eruption progressed, maximum S contents decreased and minimum Cl and F contents increased. The major, trace and volatile evolution of crystals, glass, and MI is consistent with a model that

involves either continuous or episodic recharge of the magma chamber ponded at least at 12.5 km depth.

## 1. Introduction

Development of this Doctorate was carried out in the framework of the internationalization research programme of the Ministry of University and Research (MIUR) between the Università degli Studi di Napoli "Federico II", Dipartimento di Scienze della Terra (Advisor Prof. B. De Vivo) and the Virginia Polytechnic Institute and State University, Department of Geosciences (Advisor Prof. R.J. Bodnar). The Members of the American PhD committee are: Prof. Benedetto De Vivo, Prof. Robert J. Bodnar, Prof. Annamaria Lima, Prof. Donald J. Rimstidt and Prof. Robert J. Tracy.

In the Campanian Plain, oldest volcanic products are related to ignimbrites dated from > 300 ka to 19 ka (De Vivo et al., 2001; and Rolandi et al., 2003), which according to the latter authors are not related to Campi Flegrei (CF), but are associated with fissural explosions, related to the opening of the Tyrrhenian Sea and forming of the Campanian Plain. The Phlegrean Volcanic District (PVD), Italy, (also known simply as Campi Flegrei) is one of the largest and longest-lived active volcanic complexes on Earth. The PVD comprises three volcanic fields: the CF caldera and the islands of Ischia and Procida (Fig. 1a). The PVD contains many volcanic centers (cinder cones, tuff rings, calderas) and has experienced intermittent volcanic activity for at least 50 ka with the most recent eruption being the Monte Nuovo eruption in 1538 AD. Some of these eruptions have been highly explosive, but a wide range in eruptive styles is suggested by the volcanic deposits (Table 1). Because of its location near Naples, Italy and the towns surrounding Pozzuoli Bay (1.5

million inhabitants), it is imperative to develop a better understanding of the history of the PVD system in order to better assess potential volcanic hazards associated with this active volcanic system (Fig. 2).

Melt inclusions (MI) are small samples of silicate melt which, during magma crystallization processes, are entrapped in precipitating minerals. In the last decades, MI technique has been used as a valid tool to establish the magmatic evolution (Sobolev and Shimizu, 1993; Kamenetsky et al., 1995; Frezzotti, 2001; Schiano, 2003; De Vivo and Bodnar 2003; Student and Bodnar, 2004; Kent 2008). It is now widely recognized that MI entrapped in phenocrysts in volcanic rocks can provide information concerning pre-eruptive evolution of the magma chamber (c.f. Anderson, 1976; Lowenstern, 1994; 1995; Sobolev, 1996; Wallace et al. 1999; Kent, 2008; Métrich and Wallace, 2008), assuming that MI have not been compromised following entrapment. Importantly, MI is the best tool to detect volatile concentrations before an eruption. Thus, MI is the best source of information concerning minimum depths at which the magmas were generated or evolved, and if magma was saturated in volatiles prior to an eruption. As described by Lowenstern (1994), evidence for fluid-saturation and degassing prior to an eruption can be supported from MI study. This author notes that *"saturation pressure can be calculated by incorporating volatile solubility models for the composition of interest as a function of temperature and pressure (Holloway and Blank, 1994)."* Burnham (1979) pioneered $H_2O$-silicate melt solubility model. In a recent review of volatile solubility models for silicate melts, Moore (2008) describes their application for interpreting $H_2O$ and $CO_2$ contents in MI. Métrich and Wallace (2008) report that exsolution of major volatile constituents exerts a strong control on ascent, dynamics and eruption of magmas. For instance, Webster et al. (2001),

Webster et al. (2003), and Webster et al. (2009) determined volatile contents ($H_2O$, $CO_2$, Cl, F, S) of MI from the Mt. Somma-Vesuvius system and found a correlation between the $H_2O$ and Cl abundances of the MI and the type of eruption (Fig. 3). MI in explosively erupted pumice generally had a higher $H_2O$ content than MI in more passively erupted scorias and lavas. Moreover, they report that the more explosive pumice-forming eruptions are associated with magmas that are enriched in $H_2O$, Cl and S, whereas more passive eruptions are associated with magmas with lower $H_2O$ content and lower S/Cl ratios. Worthy of note, some studies have noted that MI record temporal changes in volatile composition (Anderson at al., 2000; Saito et al., 2001; Johnson et al., 2008). Saito et al. (2001) noted that MI from early product recorded greatest depths (higher $H_2O$) relative to MI from later volcanic products of the same magmatic system. Other authors have found that volatile contents recorded by MI in olivine decrease with magmatic evolution. Thus, MI entrapped in high Fo-olivine show higher volatile contents than those entrapped in low Fo-olivine (Benjamin et al., 2007; Wade et al., 2006).

In addition to hazards associated directly with volcanic eruptions, the CF area continues to undergo episodic slow vertical deformation (bradyseism) that has been active for at least 2000 years. In 1538 the ground rose ca. 7 m immediately preceding the Monte Nuovo eruption. Thus, an understanding of the volatile history of the Campi Flegrei magmatic system will not only improve our understanding of the chemical evolution of the magmas, but will also lead to a better understanding of the relationship between crystallizing, volatile-rich magmas and surface deformation in volcanic areas.

The goal of this paper is to define the geochemical evolution of the magma associated with the Solchiaro (14.1-19.6 ka) eruption in the volcanic field of Procida. I reconstruct the

geochemical evolution studying MI. In this part, I provide new geochemical data of the magma associated with the Solchiaro eruption by MI entrapped in olivine phenocrysts. Mineral chemistry of hosting phase plus glass embayment and rim glasses are also investigated. This is an extension of what so far have been done on this eruption by other authors (Di Girolamo et al., 1984; D'Antonio et al., 1999; Cecchetti et al., 2001; De Astis et al., 2004). MI were studied in olivine from 4 representative samples of this eruption. Solchiaro products were collected to test for geochemical variations as a function of stratigraphic height and distance from the vent. This study is focused mainly on the pre-eruptive volatile concentrations. Also, the correlation among volatiles, major and trace elements, and stratigraphic height (time) is presented.

## 2. Geology and Geochronology of the Campi Flegrei (Phlegrean Field) Area

Campi Flegrei is located near the margin of the Campanian Plain (few km far from the Somma-Vesuvius volcanic apparatus) and is part of a more widespread Plio-Quaternary volcanic event that occurred in the circum-Tyrrhenian area (Peccerillo, 1999). The Campanian Margin is located in the hinge zone between the eastern Tyrrhenian Sea and the southern Apennines. Campanian magmatism is associated with NW-SE and NE-SW trending normal faults (Ippolito et al., 1973; D'Argenio et al., 1973; Finetti and Morelli, 1974; Bartole, 1984; Turco et al., 2006). The PVD includes three volcanic fields that are thought to be part of the same magmatic system: the Campi Flegrei caldera and the nearby islands of Ischia and Procida (Fig. 1).

The origin of the CF caldera, whose boundaries have been identified by gravimetric, magnetic, and seismic methods (Barberi et al., 1991; Zollo et al., 2003), is still the subject

of scientific debate. Most geologists agree that a caldera was formed by the eruption of Neapolitan yellow tuff (NYT) at 14.9 ka (Deino et al., 2004). On the other hand, there is less agreement concerning the origin of the major eruption of the Campanian Ignimbrite (CI). The CI represents the largest volume of volcanic rock in the CF area (150 $km^3$ DRE; Fisher et al., 1993). The CI is phonolitic and has been dated by De Vivo et al. (2001) and Rolandi et al. (2003) at 39 ka. According to Rosi and Sbrana (1987) and Orsi et al. (1996), the CI was erupted from a vent located in the center of the CF caldera, even though there is no clear geophysical, structural, or stratigraphic evidence supporting this interpretation. Scandone et al. (1991) suggest that the CI represents a unique event that originated from a completely different area, the Acerra Depression, northeast of CF. Based on new geochronological data, De Vivo et al. (2001) and Rolandi et al. (2003) reported that the Campanian Plain has experienced continuous, episodic ignimbrite events spanning from > 300 ka to 19 ka. The events dated at ca. 120 ka and 19 ka on land are in agreement with tephrostratigraphic data in Mediterranean Sea (Paterne and Guichard, 1993). De Vivo et al. (2001) and Rolandi et al. (2003) attribute to such events a fissural origin related to distensive faults activated along the Campanian Plain during the opening of the Thyrrenean Sea in the last 500 ka. Open problems remain the larger scale magmatic history of this region and the specific role of regional faults in controlling the location of ignimbrite eruptions (Milia and Torrente, 2007, and references therein). Cl solubility from MI from the CI indicates pressure of crystallization between 50 and 100 MPa (Signorelli et al., 2001). For the same volcanic products, Marianelli et al. (2006) using $H_2O$ solubility model estimates pressure of crystallization between 40 and 150 MPa in agreement with the formers authors. Webster et al. (2003) studied various Ignimbrites in the Campanian Plain

spanning from 205.6 ka to 23-18 ka based on MI hosted in clinopyroxene. They recognized two different populations of MI from CI: the high-Mg MI and the low-Mg MI. Also, the former group shows high contents of $H_2O$. The same two populations are observed in the Giugliano Ignimbrites (23-18 ka; De Vivo et al. 2001) and are considered to share the same or similar origin with the CI (Webster et al. 2003).

The oldest documented volcanic products in the CF area are about 50 ka and include pyroclastics and lava domes that are found only on escarpments (Alessio et al., 1973; Cassignol and Gillot, 1982; Pappalardo et al., 1999). The composition of these oldest units is trachytic and alkali-trachytic (Fig. 4: pre CI).

Pappalardo et al. (1999) recognized several pyroclastic deposits and lava domes erupted after the CI (post-CI in Fig. 4). Geochronological (Alessio et al., 1973; Scandone et al., 1991; Pappalardo et al., 1999) and stratigraphic data (Orsi et al., 1996) suggest that these formed during a period of moderate eruptive activity between 37 and 16 ka, in agreement with tephrostratigraphic data from the central Mediterranean Sea (Paterne and Guichard, 1993). These explosive-volcanic products have alkali-trachytic to trachytic composition.

The most studied eruption in the PVD, owing to its wide distribution (1000 $km^2$) and volume (40 $km^3$ DRE; Orsi et al., 1992; Wohletz et al., 1995), is the NYT (Di Girolamo et al., 1984; Rosi and Sbrana, 1987; Civetta et al, 1997; Orsi et al., 1995; Scandone et al., 1991). The NYT eruption resulted in the formation of CF caldera. The NYT products range in composition from alkali-trachytic to latitic. The NYT has been subdivided into a lower member (LM) and upper member (UM). The volcanic vent of the LM products is located in the central part of the CF caldera and the UM products originated from fissure explosions

related to the CF caldera formation. Deino et al. (2004) reported an age for NYT of 14.9 ka, determined by $^{40}Ar/^{39}Ar$. The eruption style changed with time, with earlier mostly phreatoplinian eruptions evolving into later phreatomagmatic and magmatic style eruption.

The PVD also includes the islands of Ischia and Procida that are located just west of CF. Volcanic activity at Ischia began before 150 ka (Gillot et al., 1982; Poli et al., 1987) and the latest eruption occurred as recently as AD 1302. The volcanic history is dominated by the eruption of the Mt. Epomeo Green Tuff at about 55 ka (Gillot et al., 1982). Continued episodic seismicity (Casamicciola earthquake in AD 1883), widespread fumaroles and thermal springs indicate that the magmatic system is still active.

At Procida, volcanic activity began at least as early as 55 ka, with the emplacement of the Vivara tuff (Rosi et al., 1988), and terminated with the Solchiaro eruption at about 17.3 ka (Lirer et al., 1991). Since then, no volcanic activity has been recorded, and the island contains no fumaroles and shows little seismic activity. Procida is covered by the products of later eruptions from nearby CF and Ischia (Di Girolamo and Stanzione, 1973; Rosi et al., 1988), and products of Procida eruptions occur along the mainland coast, interbedded with CF and Ischia products. The last stratigraphic study on Procida volcanites was proposed by De Astis et al. (2004; reference therein). Five volcanic vents have been recognized on the island: Vivara, Torre Murata, Pozzo Vecchio, Fiumecello and Solchiaro (from the oldest to the youngest; Fig. 5). In essence, the eruptions related to these vents provided the material to make up the actual costal line of Procida Island. The recognized volcanoes are considered to be monogenetic (De Astis et. al. 2004). The Solchiaro eruption is the most primitive (along with Vivara eruption – age is not known but is thought to be <50 ka) in composition of all of the eruptions in the PVD. Solchiaro outcrops are abundant along most

of the cost of Procida Island (Fig. 6) and in some localities reach several meters in height (De Astis et al., 2004). The style of this eruption varied through time. Early products are of phreatomagmatic origin while late products are more characteristic of magmatic origin (De Astis et al., 2004). In the last years, studies (Cannatelli et al., 2007; Cecchetti et al., 2001 and 2005; Mangiacapra et al., 2008) of primitive magmas in the PVD have been carried out using MI technique. MI from Solchiaro eruption show trackybasaltic composition and $H_2O$, $CO_2$ contents from 0 (bdl) to 3 wt% and 0 (bdl) and 4000 ppm respectively (Cecchetti et al. 2001). Minimum pressure of crystallization has been calculated from around 2 kbar to around 8 kbar (Cecchetti et al. 2001). Assuming 300 bar/km pressure-gradient, minimum depths of formation are from 27 to 7 km. Yet, Cecchetti et al. (2005) report that most of the pressures of formation by MI from MInopoli 2, Somma-Vesuvius, and Solchiaro (assuming saturation conditions) are between 2 and 4 kbar.

Sixty-four volcanic units ≤ 12 ka have been identified at CF and have been divided into 3 epochs: 1) 12-10.5 ka; 2) 8.6-8.2 ka; 3) 4.5-3.7 ka (Di Vito et al. 1999; Isaia et al., 2004). The most recent eruption occurred in September 1538 A.D. (Table 1), after 3000 years of quiescence, and formed the Monte Nuovo cone (Di Vito et al., 1987). For this eruption Piochi et al. (2005) suggest that phenocryst crystallisation occurred at $P_{H2O}$ between 1 and 2 kbar. Eruptions during the past 12 ka were mostly explosive, alternating between phreatomagmatic and magmatic phases, or were effusive and originated from monogenetic centers. The most common deposits are pyroclastic surges, ash falls, and flows, and occurred near the eruptive centers; lava domes are rare. The composition of erupted magmas ranges from trachytic to alkali-trachytic; only a few eruptions (Minopoli 1 and Minopoli 2) were fed by magmas with less evolved composition, ranging from

trachybasaltic to latitic (Armienti et al., 1983; Civetta et al., 1991; D'Antonio et al., 1999; Cannatelli et al. 2007, Mangiacapra et al. 2008). $H_2O$ contents by MI in Fondo Riccio and Minopoli 1 range from 3.25 to 6.96 wt% and from 1.93 to 5.28 respectively (Cannatelli et al., 2007). These abundances suggest a minimum pressure of formation relatively high (great depths). In a more recent study, pre-eruptive volatile contents were investigated by MI from Fondo Riccio end Minopoli 1 (Mangiacapra et al. 2008). In this study, $CO_2$-$H_2O$ systematic suggests a minimum pressure of formation mostly between 1 and 2 kbar. Roach (2005) calculates pressure of crystallization for the Agnano-Monte Spina eruption based on $CO_2$-$H_2O$ contents from MI. This author has found both $CO_2$-poor MI (0.2-0.5 kbar) and $CO_2$-rich MI (2.5 kbar).

Modern activity at CF is related to episodic slow uplift of the ground, followed by more rapid deflation (Fig. 7). This slow movement (bradyseism) represents a potential hazard to the local population, and its relationship to magmatic activity at depth was recently discussed by Bodnar et al., (2007) and Lima et al. (in press). At CF different hypotheses were proposed in order to explain ground deformation. All of the hypotheses are based on the presence of a magma body at depth. Firstly, quantitative models were obtained considering the ground deformation as a direct effect of new emplacement of magma and uplift/subsidence. Ground deformation was interpreted to be the result of elastic crust behavior in response to the magma injection (mechanical models). Later, it was proposed another hypothesis, that along with emplacement of magma into the crust, magmatic fluids injected into the whole rock plays an important role. Thus, uplift phases occurred because of high temperature fluids entering the local hydrothermal system causing overpressure into the country rock. On the other hand, once the magmatic fluid input

decreases and/or fluids exceed the country rock strength subsidence phases occur. Recently, a third way to interpret ground deformation at CF was proposed by Bodnar et al. (2007) and Lima et al. (in press). The difference between models proposed by these last authors and the previous ones is the more important role of the hydrothermal system, relative to the magma recharge. In this last interpretation of bradyseism phenomenon at CF there is the distinction of two different scale processes interacting with each other. The first process is on the order of the $10^3$-$10^4$ year, consisting of anhydrous phase crystallization of a magma emplaced at shallow depth, causing volatiles to exsolve by second boiling. The second process is on the order of decades and consists of magmatic fluids escaping from the magmatic domain and entering the overlain country rock. However, magmatic fluid failed in trespassing the low permeability cap rock (claystone and siltstone layer observed in core wells) causing ground to uplift. Eventually, the low-permeability layer begin to fracture and fluid enter into the shallow aquifers and flow to the surface determining the end of uplift and the beginning of subsidence (Fig. 5 in Lima et al., in press.). The subsidence proceeds until hydrothermal minerals precipitate and reseal the hydrothermal system.

At CF significant subsidence of the ground is best observed along the coast where ruins of medieval and Roman age show evidence of several meters of episodic vertical movement (both upward and downward). Perhaps the best-documented example of past vertical movement is at the Serapis Temple archaeological site in Pozzuoli. Boreholes left by a marine mollusk (*Lithodomus lithophagus*) on columns of this monument attracted the attention of early researchers (Breislak, 1798; Lyell, 1872), and Parascandola (1947) reconstructed the history of secular ground movements using the boreholes. This work was

later updated by reconstructing the history of vertical ground movement at CF in recent times (Dvorak and Mastrolorenzo, 1991). Radiocarbon dating of biological indicators at Serapis (Morhange et al., 2006) document three 7 m relative sea-level highstands, one during the fifth century A.D., another during the early Middle Ages, and a third in1538, when the ground rose about 7 m before the Monte Nuovo eruption. Bradyseism was again active in 1970-72, when uplift of 1 m occurred; this was followed by subsidence of 30 cm, without an eruption. Another episode of uplift of 1.8 m occurred from 1982-1984, with minor uplifts in 1988-89, 1993-94 and 2000-01. For the uplift between 1982-1984, the Bodnar et al. (2007) model indicates crystallization of 0.83 $km^3$ of $H_2O$-saturated magma at 6 km depth. Lima et al. (2009) demonstrate that the mechanical energy generated by crystallization and exsolution of magmatic fluids could lead to the recorded uplift at CF. The area entered into a new phase of uplift in 2004 that has continued to the present time (Troise et al., 2007).

Recently, seismic reflection data in the CF volcanic field revealed a geophysical discontinuity at depth of 7.5 km (Zollo et al. 2008). These authors state that a 1km thick body constituted of 80-90 % melt is present at this boundary. Also, they assume a supercritical fluid-bearing rock at ca. 3 km below the surface. Guidarelli et al. (2006) recognize under Vesuvius and the PVD a low shear velocity layer which is centred at the depth of ca. 10 km. This low velocity zone can be related to the presence of partial melting. Danyushevsky and Lima (2001) suggest, based on MI, that the two volcanic fields had shared a common origin corroborating the interpretation based on geophysical data. 3D modelling of residual aeromagnetic anomalies (Orsi et al., 1999) of the PVD reveals several magnetized bodies between 2 and 10 km, beneath Procida Island. These bodies are

interpreted to be solidified gabbroic plutons. Early studies in the near Somma-Vesuvius (SV) volcanic system, Belkin et al. (1985) and Belkin and De Vivo (1993) estimate pressures between 0.9 and 3.5 kbar, and from 1 to 2.5 kbar respectively based on fluid inclusions from ejected nodules. Cortini et al. (1985) calculated trapping depths from ca. 4 to ca. 12 km studying the same Vesuvian ejecta of Belkin et al. (1985) based on both $CO_2$ density in fluid inclusion and homogeneization temperature of coexisting silicate melt inclusion. Later, pressure of crystallization up to 6 kbar from $CO_2$-$H_2O$ fluid inclusions in 1944 Vesuvius eruption are found by Marianelli et al. (1999). For the same volcanic system, geophysical data confirmed earlier results based on fluid inclusion techniques indicating a low velocity zone between 7 and 11 km (Auger et al., 2001; Natale et al., 2005; Nunziata et al., 2006). As reported above, suggested depths associated with both the PVD and the SV overlap.

## 3. Sampling

During the Doctorate (2005-2009) 15 volcanic units from the PVD were sampled (Tab.1, units with orange background). For this study I focused on the volcanic unit of Solchiaro (14.1-19.46 ka, Alessio et al., 1976). I decide to select this eruption for 3 reasons: 1) along with Vivara eruption, it is the most primitive in chemical composition of all of the PVD. 2) Solchiaro products outcrop along most of the cost of the Procida Island and in some localities it reaches several meters in height of exposure (De Astis et al., 2004; Rolandi, personal communication). 3) The style of this eruption varied with time. Early products are of phreatomagmatic origin while late products are more characteristic of magmatic origin (De Astis et al., 2004). Other samples (NYT, Bacoli, AMS, Solfatara,

Astroni and Fossa Lupara) are not sufficiently studied to be included in the present thesis, only preliminary results have been obtained thus far. The studies on MI from these eruptions will be further detailed and the results will be used for later works. Four representative samples (RESC2, RESC3, RESC4, RESC5) of the Solchiaro eruption were collected to test for geochemical variations as a function of stratigraphic height and distance from the vent (Fig. 5 and 6). RESC2, RESC3 and RESC4 consist of ~ 20 cm of base surge deposits of the Solchiaro eruption. The collected volcanic products are poorly consolidated. The three samples consist mainly of gray ash, dark brown lapilli and phenocrysts of olivine and clinopyroxene always rimmed by glass. The samples also contain xenocrysts of sanidine that size is always around or less than 1 mm but larger than 0.5 mm showing euhedral morphology and rare pale green glass shards that are not vescivulated. Xenoliths make up less than ca. 3 % for RESC2 and RESC3 and are basically absent for RESC4. Olivine varies from 2.5 to 1.5 mm and clinopyroxenes range from 2 mm to 1 mm. A simplified chronostratigrafic correlation among samples is illustrated in figure 5. RESC2 was collected from the base of the South East cliff between Punta Pozzacco and Coricella (Fig. 5) at Procida Island ~ 2 km far from the vent (center of the Solchiaro Bay). In the outcrop, the volcanic deposit shows a sand-wave facies. RESC3 was collected 6 meter up from RESC2 and ~ 500 m closer to the vent location. RESC4 was sampled at the same distance from the vent but 15 m higher than RESC3. The latter 2 samples were collected where the base surge deposits show a characteristic plano-parallel stratification. RESC5 is representative of the yellow tuff facies, characteristic of lower and proximal products of the Solchiaro eruption (Di Girolamo et al., 1984; De Astis et al., 2004). The lithification processes obliterated the stratigrafic elements and complicated the

chronostratigraphic correlation between this sample and the others. RESC5 shows high proportion in lithic, suggesting a more phreatomagmatic eruptive style. Phenocrysts from this sample are the same size as those of the sample previously described.

## 4. Analytical methods

Olivine phenocrysts were hand picked from the poorly consolidated sample under a binocular microscope (Fig. 8 A and C) and then cleaned in deionized water with ultrasound. RESC5 was gently crushed to release crystals, and olivine phenocrysts were treated as described above. Selected crystals were mounted on glass bars (2.5 mm in diameter) with *c* axes ca. perpendicular to the section, and polished as described in Thomas and Bodnar (2002) using alumina powder, in order to prevent from carbon contamination. For each crystal, the first grinding and polishing was made to remove the first 2-10 μm of crystal/glass. The same process of grinding and polishing was repeated on the reverse side of each polished crystal to improve the visibility under the optic microscope. In this way, we increased the chances of finding more suitable MI to study. After this stage, the crystals were removed from glass bars and MI were studied petrographically (Tab. 2) under transmitted light microscope. The selection of MI was based mainly on size (> 20 μm) due to the minimum spot size suggested for Secondary Ion Mass Spectroscopy (SIMS) analyses. MI containing only glass were preferred to those containing one or more bubbles or associated crystals. Once a suitable MI was selected and studied petrographically, crystals were remounted on the glass bar. In order to maximize time,the crystals were attached at the further point from MI. When 20-25 MI were exposed, phenocrysts were removed once again from the glass rod and mounted in an indium probe mount of one inch

in diameter. Phenocrysts and glasses were mounted in indium in order to prevent $H_2O/CO_2$ epoxy contamination at high vacuum of the SIMS (Shimizu, personal communication). Each mount, containing up to 30 crystals and glassy lapilli, was analyzed using a variety of techniques. Indium mounts were coated with gold because of eventual contamination of C in MI micro fractures. MI were first examined on the scanning electron microscope (SEM; at Virginia Tech Department of Geosciences, Blacksburg VA, USA) to test for homogeneity of the glass in the MI, to look for evidence of crystallization on the inclusion walls, and to investigate for zoning of the host phase (Fig. 9 and 10). Next, the MI, glass rim, and adjacent olivine were analyzed using an electron microprobe to determine the major element chemistry. A first set of MI, glass embayment and olivines were analyzed by a Cameca SX-50 electron microprobe analysis (EPMA) for major elements at the USGS (Reston VA, USA; Tab. 3 and 5). An accelerating voltage of 15 kV was used with a beam current of 10 nA. For each MI, the host phase was analyzed >15 μm distant from the glass/host interface. Then, the same set of MI and glass were analyzed by a SIMS Cameca IMS 1280 for volatiles at the Woods Hole Oceanographic Institution (Woods Hole, MA, USA). Analyses were performed using a $^{133}Cs^+$ as the source, with a current between 1 and 1.6 nA. Glass was rastered over a 30 μm x 30 μm spot for 240 seconds to clean the surface before the sputtering. A 15 μm x 15 μm spot from each glass was analyzed ten times in depth profile mode. One MI was analyzed twice to test for homogeneity of volatile composition. Calibration curves were used to determine the concentration of volatiles using standards. Volatiles contents were related to the ratio of a given element to $^{30}Si$ (where element stand for $^{16}O^1H$, $^{12}C$, $^{19}F$, $^{32}S$, or $^{35}Cl$). A second set of phenocrysts, rim glasses, embayments, and MI were analyzed by EPMA and SIMS at Virginia Tech (Tab. 3 and 5).

Instrumental conditions for both EPMA and SIMS were mantained the same as for the first dataset. Most of the MI were analyzed twice or three times to test for homogeneity in the glass. When large enough, MI were analyzed two or three times by SIMS. For EPMA analysis, relative precision is always less than 5% one-sigma when the oxide presented a concentration larger than 1 wt%. When the concentration of an oxide was <0.1 wt% one-sigma is as large as 50%. Relative precision for volatiles by SIMS is something debatable and is not still clear, but should never be more than 10% relative for all the volatile considered (Shimizu, personal information). In addition, all MI and few olivine were analyzed by Laser Ablation Inductively Coupled Plasma Mass Spectrometry (LA ICP-MS) at the Department of Geosciences, Virginia Tech. The facility consists of a Geolas™ Pro ArF 193 nm excimer laser coupled with an Agilent 7500ce ICPMS quadrupole mass spectrometer equipped with a reaction cell. Analytical conditions for the analyses of the NIST glass, MIs, and host analyses was 27 kV, 150 mJ, with a pulse rate of 5 Hz. Precision is estimated at < 10% on the analyzed elements based on repeated analysis of NIST612 (SRM) analyzed as unknown. For LA ICP-MS analyses, NIST 610 glass was used as standard for data reduction. 60 seconds of background signal before analysis were collected before the laser was turned onto the glass or olivine. Only MI already exposed to the surface were analyzed. Thus, the laser ablates through the MI until the host phase was approached. While operating, this transition was determined monitoring elements with extremely low or high partition coefficient in the melt-olivine system (e.g., Ba, K, Na, Ni, Mg). The analytical software AMS (Mutchler et al., 2007) was used to reduce the data from the LA ICP-MS. All the element concentrations were calculated using Si as an internal standard known from EPMA analysis. Care needs to be taken for Cs contamination using

SIMS that results in a continuing change of the signal intensity with time for this ion. 500 g for each sample was treated for analysis with X-ray fluorescence spectrometry (Tab. 4).

## 5. Results

*Mineral chemistry*. Olivine compositions from all 4 samples of Solchiaro eruption range from $Fo_{79}$ to $Fo_{90}$ with Fo mol% calculated considering also the Mn and Ca components (Tab. 3). 10 olivine phenocrysts were selected and studied from sample RESC2 and their composition varies from $Fo_{82}$ to $Fo_{88}$. Most of the olivines show from euhedral to sub-euhedral shape and 3 of them present a characteristic hollow shape (see Fig.10 A and B). Olivine RESC-O22 and RESC2-O12 are strongly reverse zoned with the former showing $Fo_{82}$ on the core and $Fo_{86}$ on the rim (see Fig. 10 C and D). Chromite is a common solid inclusion in high forsterite olivine. In the case of O12 (reverse zoned) a chromite crystal is in equilibrium with the olivine and glass rim (Fig. 10 D). Often, chromite inclusions show a film of glass at the inclusion/olivine interface. 25 olivines, selected from sample RESC3, range from $Fo_{89}$ to $Fo_{77}$. These phenocrysts are either zoned or not zoned. Olivines from this sample show oscillatory, normal, and reverse zoning indicating crystallization under open system conditions or variation of oxidation state of the system during magmatic evolution. Most of the olivines have euhedral to sub- euhedral habit (Fig. 9) that indicates slow growth rate (Faure and Schiano, 2005) and glass reentrance are less frequent respect to RESC2. 17 olivines from RESC4, ranging from $Fo_{88}$ to $Fo_{79}$, also present zoning. Most of the olivines show oscillatory zoning and only few of them are not zoned. For sample RESC5 were selected 28 olivines that show the highest proportion of euhedral crystals among the Solchiaro samples. These phenocrysts rarely

show glass rim and their sizes are slightly larger than olivines from other samples (up to 3 mm). Olivines from RESC5 also show oscillatory, normal and reverse zoning. Fe-rich olivine is found in all olivines at the rim with a width of ca. 1 μm. The same Fe-rich olivine band with the same width is observed at the interface between MI and host. In addition to chromite inclusion, diopside and plagioclase inclusion were also found in few olivines.

*Melt inclusion petrography*. Studied MI are always naturally homogenized glass some contain one or more bubbles and some others contain no bubbles (Fig. 8; photo B). Size (1 up to 400 μm in diameter) and colour (colorless to brownish) are both variable with larger inclusions being more brownish than smaller ones. Colour tone of MI is dependent on MI thickness as suggested by its correlation with size. Proportion of MI containing only glass increases from earlier to later volcanic products (from RESC2 to RESC4). Unfortunately, when melt inclusion assemblage (MIA) was observed, MI size (<3 μm) was not suitable for this study. Thus, there are no ways to test if two different MI were entrapped at the same time. When it was possible we studied more than a single MI in the same unzoned phenocrysts to test for geochemical variation among MI entrapped in *similar* physical conditions. Shape is variable ranging from perfectly elliptical/spherical through faceted (negative shape of olivine) to irregular (Tab. 2). In some crystal MI show constant $V_{melt}/V_{bubble}$ ratio (e.g. RESC3-O6) whereas in some other the same ratio is highly variable (e.g. RESC4-O10). I noted that for some olivines MI do not contain bubble below a precise size. For instance, MI in olivine RESC3-O9 <50 μm do not contain any bubbles. Other olivine phenocrysts show in one sector that MI contain no bubble while in another sector MI contain bubble with constant $V_{melt}/V_{bubble}$. Only in one case, the later ratio is less than 0.7 (RESC3-O3). This strongly suggests that glass is often entrapped as a single phase, and

that bubble is just due to post-entrapment variation of physical (shrinkage bubble) or chemical (crystallization on the wall of olivine) conditions. The host/inclusion interface is often smooth at the μm scale. In few cases this interface show wrinkled texture that is also found in some reheated MI in laboratory and may indicate natural reheating. MI, from all the Solchiaro samples, are often associated with chromite solid inclusions (mixed MI; Roedder, 1979). The $V_{melt}/V_{chromite}$ ratio ranges from 1 to close to 0 that indicate chromite is not a daughter crystal. In fact, sometimes the MI appear to have nucleated on the chromite crystal face. Bubbles in mixed MI is always attached at the chromite inclusion. In 2 cases MI are associated with clinopyroxene.

*Open glass.* For *open* glass I identify every glass in contact with olivine but not included into it. In other words, open glass are all glasses, but not those from MI. Under this category I consider embayment that are connected through one or more narrow decks to the outside, glass reentrants, glass rim, and highly vesciculated glasses (lapilli). Glass embayment often show irregular shape and in some cases are connected to the outside through more than one neck of various width. Bubbles are often found in glass embayment, but never attached on the host wall. This is also observed in glass rim and glass reentrants where bubbles are always found far from the rim of the phenocrysts in some cases as distant as ~50 μm. When under the optic microscope bubbles appear to touch the olivine walls, BSE petrography reveals that bubbles are not attached directly to the olivine wall, but to plagioclase or clinopyroxene microphenocrysts at the olivine melt interface (Fig. 11).

Generally, bubble size increases with increasing distance from the olivine rims and varies from 500 μm to 5 μm in diameter. Most of the bubbles show spherical shape, but especially in sample RESC3 and RESC4, there are some cases with more ellipsoidal shape.

Microphenocrysts of plagioclase, diopside, olivine, and chromite in order of abundance are observed in open glass. Note that plagioclase is never found as phenocryst and is always less than 150 μm while diopside is present as both microcryst and phenocryst. Generally, plagioclase and clinopyroxene show baby swallowtail morphology developed on tabular morphology. Only in few cases clinopyroxene show skeletal and dendritic morphology.

*Major element*. MI composition may show strong disequilibria with the adjacent host phase. In fact, MI composition could have been modified by post entrapment crystallization (PEC) (Kent. 2008, reference therein). Thus, chemical compositions of MI were corrected for possible PEC. I recalculated compositions using petrolog software by Danyushevsky. In order to run the software I choose for this system oxidation state as the NNO buffer that is suggested for the nearby Roman magmatic province by Métrich and Clocchiatti (1996). The software calculated the ratio $Fe^{2+}/Fe^{3+}$ based on Borisov and Shapkin 1990 equation. Olivine-silicate melt equilibrium was determined based on Ford et al. (1983) thermobarometric equations and pressure was set to 1 bar (there is no significant variation in composition considering different pressure up to 4 kbar). All calculations were made assuming anhydrous system and were normalized to 100% (Tab. 5). Obviuously, open glasses were not corrected. As can be noted from table 3 the percentage resulted from the correction is never higher than 10%. Thus, the correction does not strongly affect the uncorrected MI composition.

Corrected MI and glass composition plot on the fields from basalt through trachy-basalt to basaltic trachy-andesite with few points on the phono-tephrite based on TAS diagram by Le Bas et al. (1986) as shown in figure 12. Bulk rock analyses plot in the trachy-basalt field and show more evolved composition relative to some compositions from

MI. In sample RESC2 open glasses show slightly less evolved compositions than the bulk rock. This is indicative of open system magmatic processes corroborating the hypothesis of a slightly less evolved magma recharging, also in agreement with petrographic evidence. All glass compositions are nefeline-normative. Since MI composition was corrected based on host composition, there is a strong positive correlation between Mg# and Fo mole % of olivine (Fig. 13). As also shown by most of the petrological studies based on MI, composition of the latter span a wider range in major/trace element, volatile, and isotope relative to both bulk rock and matrix glass (Fig. 12 and 14). In figure 14, Mg# decrease with decreasing $CaO/Al_2O_3$ ratio. This suggests that along with olivine also diopsidic clinopyroxene is crystallizing in agreement with hand specimen observation. The most variable major element concentration of corrected MI is $K_2O$ (from 0.5 to 6 wt%, see Fig. 15). This is a variation that is also found for whole rock analysis from Solchiaro eruption (De Astis et al, 2004) and also for MI from Roman Province (higher values; Kamenetsky et al., 1995). Other major elements span a wide range (e.g. CaO, FeO and $TiO_2$). Based on $K_2O$ contents I subdivided MI in 2 groups: $K_2O$-poor MI with $K_2O < 2$ wt%, and $K_2O$-rich MI with > 2 wt%.

*Trace element.* Trace elements in MI were also corrected for PEC. Trace elements contents from $K_2O$-poor MI are significantly different relative to $K_2O$-rich MI, as can be observed from figures 16 and 17. In particular, the former group compositions show Sr and Eu positive anomaly typical of plagioclase composition. Generally, incompatible trace element in $K_2O$-poor MI show lower contents respect to $K_2O$-rich MI with the exception of Sr, Y and Yb (Fig. 17). Open glasses and bulk rock composition both from this work and literature show same distribution as $K_2O$-rich MI. REE of $K_2O$-poor MI show gradually

flatter distribution with decreasing $K_2O$ content. The lowest $K_2O$-MI presents quasi-flat distribution with slight enrichment in lighter and heavier REE. Since REE distribution is not affected by crystal fractionation, the signature from $K_2O$-poor MI is either related to different source or to assimilation from the crust. On one hand, LILE distribution of $K_2O$-poor compositions resemble the one obtained by lower crust average for more incompatible trace elements (up to Nd; see Fig. 17). On the other hand, HFSE have no matching with the lower crust distribution, but have almost the opposite behavior (Fig. 17).

*Volatiles.* Volatiles in MI were corrected for PEC. $K_2O$-poor MI show the lowest contents for $CO_2$, S, Cl, and F. As can be observed from figure 18, the highest content of $CO_2$ is in sample RESC2 that is the earlier volcanic product that I collected followed by RESC5, RESC3 and RESC4. In addition to $CO_2$, open glasses show the same results for S contents. Thus, the sample at the top of the stratigraphic column contains open glass with lower maximum S concentration. The lowest F and Cl contents are characteristic of open glass from sample RESC4. $H_2O$-$CO_2$ concentrations of all glasses from all samples fit a calculated degassing path for a saturated basaltic magma (Newman and Lowenstern, 2002; Fig. 19). Maximum pressures of formation calculated from volatilecalc software from the latter authors are 3.5 kbar. The narrow interval of $H_2O$ contents from MI (from 0.9 to 1.7 wt%) suggests an open system degassing. The degassing path reported in figure 19 is calculated assuming 1200 ºC isothermal condition, $SiO_2$ concentration is set at 49 wt%, and starting concentrations of dissolved $H_2O$ and $CO_2$ are 1.25 wt% and 2000 ppm respectively. Open glass contents also follow the same degassing path, but they extend down to lower concentration of $H_2O$ and a more closed system behavior with up to 10 % initial gas phase. If samples are considered separately maximum depths recorded by glass compositions are

greater in sample RESC2 followed by RESC5, RESC3, and RESC4. Therefore, there is a relationship between stratigraphic height and maximum $CO_2$ concentrations from different samples. Minimum pressures of crystallization are around 200 bars for all the samples. Except for $H_2O$-$CO_2$ plot, other couples of volatiles do not show any correlation for MI. On the other hand, couples of volatiles in open glass always show unequivocal trends (Fig. 20 and 21). For instance, $H_2O$-S contents also fit degassing paths for open glass (Fig. 20). Once again, maximum $H_2O$-S concentrations are recorded by open glass from earlier volcanic products. Thus, maximum S contents decrease with stratigraphic height. The reverse behavior is detected for Cl and F, still considering open glass compositions. Minimum Cl and F show lower concentrations in the earliest erupted sample (RESC2) and higher minimum concentrations in the latest volcanic product sampled (RESC4; Fig. 21). As observed from figure 21 and 22, Cl spans in a wider range than F in agreement with the more solubility in silicate melts of the latter respect to the former. In the triangular diagram $H_2O$-F-Cl, MI and open glass show slightly different trends (Fig. 22). Glasses in the triangular diagram $H_2O$-$CO_2$-S indicate that $CO_2$ is the less soluble volatile followed by S and $H_2O$. This is consistent with experimental data where first fluid exsolving from magma are $CO_2$-rich. Figure 23 may indicate that once $CO_2$ reach a certain value S starts to exsolve and the fluid in equilibrium with the melt decreases in its $CO_2$ content and increases in its S content. That may explain the reason why in MI simple correlation between 2 volatiles is not observable.

## 6. Discussion

The overlapping shown in the $CaO/Al_2O_3$ versus Mg# plot of MI compositions with those of bulk rock (from both this study and literature) suggests that corrected MI compositions are representative of the Solchiaro magma, the Procida Island magmatism, and the whole PVD. Size of MI versus $K_2O$ plot shows that as the size increases the $K_2O$ content approximates the one from bulk rock analysis and that for smaller size $K_2O$ spans in a wider range (Fig. 24). Size reported in figure 24 was calculated before each MI was exposed to the surface for analysis. For calculated size, I mean the area of a sphere or an ellipse (depending on the shape of MI) when most of the inclusion wall was on focus under the optic microscope. When $K_2O$ concentrations are higher than the bulk rock concentrations, one possible explanation is that MI was modified by boundary layer effect. In fact, this major element is incompatible with mineral phases crystallizing in this system. However, MI also show lower contents that are in contrast with this hypothesis. The large interval of $K_2O$ concentration is not consistent with fractional crystallization since this would require also other major elements to undergo to such huge variation (e.g. MgO and CaO). Other incompatible elements (P, Sr, Rb, and Ba) plotted versus MI size show the same distribution (Fig. 24). My interpretation of this distribution is that MI sampled small scale heterogeneity of the melt from which the host phase is growing. This is in agreement with what Kent (2008) notes "…*The volumes of individual eruptive units in basaltic volcanoes vary, but even the smallest eruptions are many, many orders of magnitude greater in volume than individual melt inclusions, which rarely exceed a few thousand cubic microns. Erupted lava or tephra compositions are thus considered to represent blended mixtures of a number of different melt compositions, whereas melt inclusions*

*sample this diversity at a smaller scale, consistent with their smaller volumes and protect trapped melts from subsequent mixing and blending.*"

Moreover, in figure 25 $Al_2O_3$ versus CaO plot show MI overlap with bulk rock compositions that suggests MI were entrapped during slow growth rate as also indicated by the polyhedral morphology of most of the olivine in which MI are hosted (especially RESC5 sample). That corroborates the hypothesis that corrected MI compositions are representative of melt from which the host phases are growing. In fact, Faure and Schiano (2005) conclude that MI in polyhedral olivine are the most suitable because only in this case there is no large enrichments in $Al_2O_3$ over CaO (in the CMAS system) due to diffusion at the glass/olivine interface.

As reported in the results of this study, chromite associated with MI are not considered to be daughter mineral. Firstly, the ratio $V_{melt}/V_{chromite}$ varies from 1 to almost 0. Secondly, Cr contents from some MI that contains only glass show the same concentration in respect to some other MI associated with chromite inclusion.

One of the concerns studying MI is to establish if its dissolved volatile content represents that at the moment of the entrapment, especially for MI containing bubble. In addition to PEC, part of the volatile content may be transferred to the "vapor" phase (bubble included into the MI). Since $CO_2$ is the least soluble among volatiles one should expect a $CO_2$-rich fluid coexisting with the glass. On one hand, $CO_2$ in some of the selected MI was detected in the bubble by RAMAN spectroscopy. On the other hand, if MI with the same interval of CaO/ $Al_2O_3$ ratio are considered, there are MI containing bubble that have equal $CO_2$ concentration relative to other MI containing only glass. Moreover, thermometric experiments performed by the author on MI containing bubble show no

change of phase into bubble. If I assumed the fluid consists only of $CO_2$, the density of the fluid is always extremely low because the liquid-vapor curve is never intersected. Due to the volume of the bubble (always < 5 μm) $CO_2$ concentration of this vapor phase is never higher than few 10s of ppm. Thus, volatiles concentrations dissolved in the glass of all MI selected for this work are considered to be total contents even for MI containing bubble. Diffusion of volatiles through the host phase is also a possible source of under/sovra estimation of concentrations from MI. However, open glasses concentrations present same trends shown by those from MI. Yet, $H_2O$ loss for diffusion from MI through the host is limited by the amount of $Fe^{2+}$ available in the melt and gain of $H_2O$ for diffusion is instead limited by the $Fe^{3+}$ content of the melt (Danyushevsky et al., 2002). In addition, there is no observation based on volatile trends described above leading to the hypothesis of significant loss or gain of volatiles for diffusion.

In addition to reverse and oscillatory zoning in olivine, open glasses, showing less evolved composition than some of the studied MI, indicate that the magma underwent through open system processes such recharging from less evolved melt. This is also confirmed by previous work on Procida Island magmatism (D'Antonio et al., 1999; De Astis et al., 2004) nevertheless on the near by Mt. Etna volcano (Spilliart et al., 2006).

The lowest $K_2O$ content in melt that have been ever documented in the PVD is 1.24 wt% from a lithic contained in Solchiaro or Vivara deposits (D'Antonio et al., 1999; sample APR 18 not specified from which eruption the sample is) while the lowest $K_2O$ in scoria sample (APR 14) from Solchiaro or Vivara products reported by the same authors is 1.56 wt%. De Astis et al. (2004) report $K_2O$ content as low as 1.76 wt% for the Solchiaro eruption (sample Pro 7/11). The lowest $K_2O$ content I detected in this work is 0.51 wt% and

is from corrected MI (RESC3-O22-MA, Tab. 5).In addition, 11 MI contain less than 2 wt% in $K_2O$. Also, these $K_2O$-poor MI show $TiO_2$, $P_2O_5$ and NaO contents unusually low (RESC2-O26-M1: 0.63, 0.23, 1.94 wt% respectively, table 5) and CaO content unusually high (13.89 in RESC2-O26-M1) for the PVD. MI hosted in Fo-rich olivine (87-90 mole%) plus Cr content as much as 240 ppm suggest that some of the MI are primitive in character. All glass compositions show MgO > 4 wt% and are suitable for understanding the origin of this magma. In figure 26, Zr-Ti-Y discriminant diagrams indicate that most of the glass composition show within plate basalt affinity. This is also reported in De Astis et al. (2004) work based on major/trace elements and isotopic compositions from bulk rock analysis. They argue that the parental magma is characterized by both intraplate affinity for HREE composition and by subduction signature for LILE enrichment and immobile elements depletion. In agreement with this conclusion, 4 MI of the $K_2O$-poor MI group plot differently relative to all the other glass compositions showing volcanic arc signature. As presented in the above results also spider diagrams suggest two different kinds of magma. Around 95% of the magma is characteristic of intraplate basalt, while the other 5 % of the magma is related to active margin basalt. One possible interpretation is that Solchiaro associated magma is generated by a heterogeneous mantle source as also argued by Kamenetsky et al. (1995) whose conclusions are mainly based on the $K_2O$ large interval in MI hosted in Fo-rich olivine of the nearby Vulsini volcanic system (Roman Province). However, for Solchiaro magma the hypothesis of two different kind of parental magma is hazardous due to the not extremely primitive character of most of phenocrysts and glass. Further investigations are certainly needed on this issue. Another possible hypothesis is that the $K_2O$-poor MI represent assimilation of plagioclase-bearing lower crust. In favor of this

statement is the matching in the spider diagrams of LILE and the strong negative anomaly of Nb. However it is difficult to justify the negative anomalies of Sm, Zr, Hf and Ti. Moreover, pressures recorded from $K_2O$-poor MI are the lowest detected, suggesting that MI were entrapped at upper crust depth.

Open glass $H_2O$-$CO_2$ compositions fit closed degassing paths while those from MI fit more open degassing paths (degassing paths are calculated from Newman and Lowenstern, 2002). In fact, prior to a magmatic eruption, fluids failed to escape the system building up the internal pressure that may be lead to an explosion. Except for $H_2O$-$CO_2$, in MI other simple correlations between other couples of volatiles are not observed. These missed correlations could be due to the complexity of the multi-volatile component system (Fig. 22 and 23). It is also possible that MI volatiles (except for $H_2O$-$CO_2$) do not show correlations because they recorded magma that degassed under open condition. Therefore, under open condition S failed to degas in a systematic way whereas under closed system it degassed in similar way of $CO_2$. The oxidation state of the system may change with the passage from open to close degassing. It is well known that sulfur solubility is also controlled by the oxygen state in addition to pressure (Jugo et al., 2005).

In this study, glasses show reverse correlation between calculated maximum pressure (~ maximum $CO_2$) and stratigraphic height. S from open glass also shows maximum content in the sample RESC2 (bottom of the stratigraphic column). F and Cl correlate with stratigraphic height, but in a positive way. Saito et al. (2001) describe a similar volatile evolution for the Satsuma-Iwojima volcano in Japan. From earlier to later products calculated pressures, based on MI, decrease from earlier maximum pressure of ca. 1.7 kbar to later maximum pressure of ca. 0.75 kbar. This is interpreted to represent the magma

ascending the crust with time. The greatest pressure recorded by glasses from Solchiaro is 3.5 kbar that assuming 280 bar/km gradient results in 12.5 km depth. This is in agreement with maximum pressures estimated by Belkin et al. (1985) based on fluid inclusions from ejected nodules Somma-Vesuvius volcanic system. Also, Guidarelli et al. (2006) recognized a low velocity zone under both the PVD and the Somma-Vesuvius system at around 10 km depth that is close to max depth recorded by MI from this study. MI and open glass indicate that in earlier phase the Solchiaro magma coexisted with a vapor phase at 3.5 kbar (RESC2 sample). Sample RESC5 fit in all diagrams between samples RESC2 and RESC3 suggesting that the former was erupted later than RESC2 and before RESC3. If the hypothesis of systematic correlation between stratigraphic height and volatile contents is correct, then analysis of glasses is a useful tool to asses relative ages for Solchiaro outcrops otherwise of difficult interpretation. Glasses from a single sample record large range of depths from 3.5 kbar down to almost atmospheric pressure (RESC2) and that is difficult to interpret. However, similar large ranges have been reported from several studies based on MI (Wade et al., 2006; Benjamin et al., 2007; Johnson et al. 2008; Marianelli et al., 2006; Mangiacapra et al., 2008). On one hand, MI composition record different pressure because they can be entrapped at different time and thus at different depth of the whole plumbing system or they represent degassing at isobaric condition due to magma convection in a conduit (Kazahaya et al., 1994). On the other hand, open glasses formed at the same time and the large interval of calculated pressures needs another interpretation. As far as the author knows, no study reports such high volatile contents from “open” volcanic glass. The first possible explanation for the observed data is that open glasses were quenched also at great depth because of the high explosive eruption. The second possible

solution is that at the moment of the eruption open glasses were under super-saturation condition due to magma recharging from deeper level that triggered eruptive explosion.

Orsi et al. (1999) argued the presence beneath the Island of Procida of gabbroic bodies from 2 to 10 km possibly representing ancient cooled magmatic chamber related to the basic magmatism of this volcanic field. These bodies may also represent a continuous gabbroic dike from which the Solchiaro magma ascended the crust similar to what is modeled for Mt. Etna volcano (Spilliaert et al. 2006). The tectonic setting of the Island of Procida also fit with this interpretation.

## 6. Conclusion

Magma associated with Solchiaro eruption shows both within plate basalt and subduction related basalt imprints. These two different imprints are detected by two distinct group of MI, here called $K_2O$-rich MI and the $K_2O$-poor MI. The first group shows the same signature of bulk rock from literature and we consider it to be originated from a metasomatized mantle in a within plate setting (De Astis et al., 2004). The second group show composition never reported in the literature for the PVD and may be related to orogenic peridotite. The author argues that small MI (< 1000 $\mu m^2$) sampled and prevented from subsequent mixing small scale heterogeneity (Kent 2008) of Solchiaro associated magma. $CO_2$ is the less soluble volatile followed by S if the system is closed. Cl and F are instead retained in glass from the earlier to the later erupted products and F is slightly more soluble than Cl.

Volatile element trends are consistent with the following magmatic history as illustrated in figure 27: 1) earlier magma (RESC2) was saturated in volatiles and ponded at

12.5 km before eruption. MI and glass erupted at this stage record the greatest depths. 2) The magma chamber continuously degassed through the conduit. MI and glass from eruptive event represented by RESC3 record lower maximum contents of $CO_2$, S and $H_2O$ and higher minimum contents of Cl and F relative to those of earlier events. 3) At later eruptive phases, degassed magma contained the lowest maximum concentrations of $CO_2$, S and $H_2O$ and the highest minimum concentrations of Cl and F relative to earlier phases (RESC4).

In conclusion, greatest depth obtained from MI is consistent with recent geophysical data (Guidarelli et al., 2006) in the region. Cl and F increase with time whereas $CO_2$ and S decrease during the Solchiaro eruption. Finally, the observed major and trace element and volatile evolution of crystals, glass, and MI is consistent with a model that involves either continuous or episodic recharge of the magma chamber (petrographic evidence) at depth, combined with the degassing of magma associated with the Solchiaro eruption.

**7. Acknowledgements**

I would like to thank my sister since this thesis would have never being possible without her existence.

**8. References**

Alessio M., Bella F., Improta S., Belluomini G., Cortesi C. and Turi B., 1973. University of Rome Carbon - 14 Dates X. Radiocarbon, 15 (1): 165-178.

Alessio M., Bella F., Improta S., Belluomini G., Cortesi C. and Turi B., 1976. University of Rome Carbon - 14 Dates XIV. Radiocarbon, 18: 321-349.

Anderson A.T., 1976. Magma mixing: Petrological process and volcanological tool. J. Volcanol. Geotherm. Res., 1, 3-33.

Anderson, A.T., Davis, A.M., Fangqiong, Lu., 2000. Evolution of Bishop Tuff rhyolitic magma based on melt and magnetite inclusions and zoned phenocrysts. J. Petrol. 41, 449-473.

Armienti P., Barberi F., Bizouard H., Clocchiatti R., Innocenti F., Metrich N., Rosi M. and Sbrana A., 1983. The Phlegraean Fields: magma evolution within a shallow chamber. J. Volcanol. Geotherm. Res., 17: 289-311.

Auger, E., P. Gasparini, J. Virieux, and A. Zollo, Seismic evidence of an extended magmatic sill under Mt. Vesuvius, Science, 294, 1510– 1512, 2001.

Barberi F., Cassano E., La Torre P. and Sbrana A., 1991. Structural evolution of Campi Flegrei Caldera in light of volcanological and geophysical data. J. Volcanol. Geotherm. Res., 48 (1/2): 33-49.

Bartole R., 1984. Tectonic structures of the Latian-Campanian shelf (Tyrrhenian sea). Boll. Ocean. Teor. Appl., 2: 197-230.

Belkin, H.E., De Vivo, B., Roedder, E., Cortini, M., 1985. Fluid inclusions geobarometry from ejected Mt. Somma-Vesuvius nodules. Am. Mineral. 70, 288–303.

Belkin H. E. and De Vivo B., 1993. Fluid inclusion studies of ejected nodules from Plinian eruptions of Mt. Somma-Vesuvius. J. Volcanol. Geotherm. Res., 58: 89-100.

Benjamin E.R., Plank T., Wade J.A., Kelley K.A., Hauri E.H., Alvarado G.E., 2007. High water contents in asaltic agmas from Irazù volcano, Costa Rica. J. Volcanol. Geotherm. Res. 168:68-92.

Bodnar RJ, Cannatelli C, De Vivo B, Lima AM, Belkin HE & Milia A (2007) Quantitative model for magma degassing and ground deformation (bradyseism) at Campi Flegrei, Italy: Implications for future eruptions. Geology, 35, no. 9, 791-794.

Borisov A.A., Shapkin A.I., 1990. A new empirical equation relating $Fe^{3+}/Fe^{2+}$ in magmas to their composition, oxygen fugacity, and temperature. Geochem Int 27: 111±116.

Breislak, S., 1798. Topografia fisica della Campania. Antonio Brazzini, Firenze, Italy.

Burnham, C.W., 1979. The importance of volatile constituents. The Evolution of the Igneous Rocks; 50th Anniversary Perspective. Princeton University Press, pp. 439–482.

Cannatelli C., Lima A., Bodnar R. J., De Vivo B., Webster J. D. and Fedele L., 2007. Geochemistry of melt inclusions from the Fondo Riccio and Monopoli 1 eruptions at Campi Flegrea (Italy). Chemical Geology, 237: 418-432.

Cassignol, C., Gillot, P.Y., 1982. Range and effectiveness of unspiked potassium-argon dating: experimental ground work and application. In: Odin, G.S. (Ed.), Numerical Dating in Stratigraphy. Wiley, New York, 160 pp.

Cecchetti A., Fulignati P., Marianelli P., Proto N., Sbrana A., 2001. The feeding system of Campi Flegrei. Insights from melt and fluid inclusions on Ignimbrite Campana, Solchiaro and Minopoli eruptions. GNV-INGV Meeting, Rome, Italy, 9–11 October 2001, Abstracts vol:190–191.

Cecchetti, A., Marianelli, P., and Sbrana, A., 2005, Neapolitan active volcanoes: A study of the medium-high pressure feeding systems through melt inclusions, *in* XVIII European Conference on Research on Fluid Inclusions, Siena, Italy, University of Siena, abs. 03.

Civetta, L., Carluccio, E., Innocenti, F., Sbrana, A. and Taddeucci, G., 1991. Magma chamber evolution under the Phlegrean Field during the last 10 ka: Trace element and isotopic data. Eur. J. Mineral., 3: 415-428.

Civetta L., Orsi G., Pappalardo L., Fisher R.V., Heiken G. and Ort M., 1997. Geochemical zoning, mingling, eruptive dynamics and depositional processes - The Campanian Ignimbrite, Campi Flegrei caldera, Italy. J. Volcanol. Geotherm. Res., 75: 183-219.

Cortini M., Lima A. and De Vivo B., 1985. Trapping temperatures of melt inclusions from ejected vesuvian mafic xenoliths. J. Volcanol. Geotherm. Res., 26: 167-172.

D'Antonio M., Civetta L., Orsi G., Carandente A., de Vita S., Di Vito M.A., Isaia R., Pappalardo L. and Piochi M., 1999. The present state of the Phlegraean magmatic system in the last 12 ka. J. Volcanol. Gotherm. Res., 91: 247-268.

D'Argenio B., Pescatore T.S. and Scandone P., 1973. Schema geologico dell'Appennino Meridionale. Acc. Naz. Lincei, Quad. 183: 49-72.

Danyushevsky, L.V., Lima, A., 2001. Relationships between Campi Flegrei and Mt. Somma volcanism: evidences from melt inclusions in clinopyroxene phenocrysts from volcanic breccia xenoliths. Mineral. Petrol. 73, 107– 119.

Danyushevsky L.V., McNeill A.W., Sobolev A.V., 2002. Experimental and petrological studies of melt inclusions in phenocrysts from mantle-derived magmas: an overview of techniques, advantages and complications. Chem Geol 183:5–24.

Deino A.L, Orsi G., de Vita S., Piochi M., 2004. The age of the Neapolitan Yellow Tuff caldera-forming eruption (Campi Flegrei caldera: Italy) assessed by $^{40}Ar/^{39}Ar$ dating method. Journal of Volcanology and Geothermal Research 133: 157-170.

De Astis G., Piochi M., Pappalardo L., 2004. Procida Volcanic History: new insights in the evolution of the Phlegraean Volcanic District (Campania, Italy). Bull. Volcano.l 66: 622–641.

De Vivo B., Rolandi G., Gans P.B., Calvert A., Bohrson W.A., Spera F.J. and Belkin H.E., 2001. New constraints on the pyroclatic eruptive history of the Campanian volcanic Plain (Italy). Mineralogy and Petrology, 73: 121-143.

De Vivo B. and Bodnar R.J., 2003. "Melt inclusions in volcanic systems", Elsevier Sciences B.V.

Di Girolamo, P., Stanzione, D., 1973. Lineamenti geologici e petrologici dell'isola di Procida. Rend. Soc. Ital. Mineral. Petrol. 24: 81-126.

Di Girolamo P., Ghiara M.R., Lirer L., Munno R., Rolandi G. and Stanzione D., 1984. Vulcanologia e petrologia dei Campi Flegrei. Boll. Soc. Geol. It., 103: 349-413.

Di Vito M. A., Lirer L., Mastrolorenzo G. and Rolandi G., 1987. The Monte Nuovo eruption (Campi Flegrei, Italy). Bull. Volcanol., 49: 608-615.

Di Vito M.A., Isaia R., Orsi G., Southon J., D'Antonio M., de Vita S., Pappalardo L. and Piochi M., 1999. Volcanic and deformation history of the Campi Flegrei caldera in the past 12 ka. J. Volcanol. Geotherm. Res. 91 (2-4): 221-246.

Dvorak, J. J. & Mastrolorenzo, G. 1991. The mechanism of recent vertical crustal movements in Campi Flegrei caldera, Southern Italy. Geology Society of America, Special Paper, 263.

Faure F. and Schiano P., (2005). Experimental investigation of equilibration conditions during forsterite growth and melt inclusion formation. Earth Planet Sci Lett 236:882-898.

Finetti I. and Morelli C., 1974. Esplorazione sismica a riflessione dei Golfi di Napoli e Pozzuoli. Boll. Geof. Teor. Appl., 16 (62/63): 175-222.

Fisher R.V., Orsi G., Ort M., Heiken G., 1993. Mobility of a large volume pyroclastic flow emplacement of the Campanian Ignimbrite, Italy. J. Volcanol. Geotherm. Res. 56: 205-220.

Ford C.E., Russel D.G., Craven J.A., Fisk M.R., (1983). Olivine-liquid equilibria: temperature, pressure and composition dependence of the crystal/liquid cation partition coefficients for Mg, Fe2+, Ca and Mn. J Petrol 24: 256±265.

Frezzotti M.L., 2001. Silicate-melt inclusions in magmatic rocks: application to petrology. Lithos 55, 273–299.

Gillot P. Y., Chiesa S., Pasquarè G. and Vezzoli L., 1982. 33.000 yr K/Ar dating of the volcano-tectonic horst of the isle of Ischia, gulf of Naples. Nature 229: 242-245.

Guidarelli M., A. Zille, A. Saraò, M. Natale and G.F. Panza, 2006. Shear-wave velocity models and seismic sources in Campanian volcanic areas: Vesuvius and Phlegraean Fields. In: F. Dobran, Editor, Vesuvius: Education Security and Prosperity, Developments in Volcanology vol. 8, Elsevier, Amsterdam (2006), pp. 287–310.

Holloway J. R. and Blank J. G. (1994) Application of experimental results to C-O-H species in natural melts. In *Volatiles in Magmas* (ed. M. R. Carroll and J. R. Holloway), Vol. 30, pp. 187– 30. Rev.

Ippolito F., Ortolani F. and Russo M., 1973. Struttura marginale tirrenica dell'Appennino Campano: reinterpretazione di dati di antiche ricerche di idrocarburi. Mem. Soc. Geol. It., XII: 227-250.

Isaia R., D'Antonio M., Dell'Erba F., Di Vito M., Orsi G., 2004. The Astroni volcano: the only example of closely spaced eruptions in the same vent area during the recent history of the Campi Flegrei caldera (Italy). Journal of Volcanology and Geothermal Research 133: 171-192.

Johnson E.J., Wallace P.J., Cashman K.V., Delgado Granados H., Kent A., 2008. Magmatic volatile contents and degassing-induced crystallization at Volcan Jorullo, Mexico: Implications for melt evolution and the plumbing systems of monogenetic volcanoes. Earth. Planet. Sci. Lett. 269:477-486.

Jugo P.J., Luth R.W., Richards J.P., 2005. Experimental data on the speciation of sulfur as a function of oxygen fugacity in basaltic melts. Geochim Cosmochim Acta 69:477–503.

Kamenetsky V.S., Metrich N., Cioni R., 1995. Potassic primary melts of Vulsini (Roman Province): evidence from mineralogy and melt inclusions. Contrib. Mineral. Petrol. 120: 186-196.

Kazahaya, K., H. Shinohara and G. Saito, 1994, Excessive degassing of Izu-Oshima volcano: magma convection in a conduit, Bull. Volcanol. 56, 207-216.

Kent A.J.R., 2008. Melt inclusions in basaltic and related volcanic rocks. Rev. Mineral. Geochem. 69: 273–331.

Le Bas M.J., Le Maitre R.W., Streckeisen A., Zanettin B., 1986. A chemical classification of volcanic rocks based on the total alkali-silica diagram. J. Petrol. 27: 745-750.

Lowenstern J.B., 1994. Dissolved volatile concentrations in ore-forming magma. Geology, 22, 893-896.

Lowenstern, J.B., 1995. Applications of silicate melt inclusions to the study of magmatic volatiles. In: Thompson J.F.H. (Ed.), Magmas, Fluids, and Ore Deposits, vol Short Course, vol. 23, Minerological Association of Canada, Victoria, pp. 71–101.

Lima A., De Vivo B., Spera F.J., Bodnar R.J., Milia A., Nunziata C., Belkin H.E. and Cannatelli C., in press. Thermodynamic model for uplift and deflation episodes (bradyseism) associated with magmatic-hydrothermal activity at the Campi Flegrei (Italy). Earth Planetary Science Letters.

Lirer, L., Rolandi, G., Rubin, M., 1991. 14C age of the 'Museum Breccia' (Campi Flegrei) and its relevance for the origin of the Campanian Ignimbrite. J. Volcanol. Geotherm. Res. 48, 223-227.

Lyell, C., (1872). Principles of geology. Murray J. (Ed.), London, 164-179 p.

Mangiacapra A., Moretti R., Rutherford M., Civetta L., Orsi G., and Papale P., 2008. The deep magmatic system of the Campi Flegrei caldera (Italy). Geophysical Research Letters: VOL. 35, L21304, doi:10.1029/2008GL035550.

Marianelli P, Métrich N, Sbrana A (1999) Shallow and deep reservoirs involved in magma supply of the 1944 eruption of Vesuvius. Bulletin of Volcanology 61: 48-63.

Marianelli P., Sbrana A., Proto M., 2006. Magma chamber of the Campi Flegrei supervolcano at the time of eruption of the Campanian Ignimbrite. Geology 34(11):937–940.

Métrich N., Clocchiatti R., (1996). Sulfur abundance and its speciation in oxidized alkaline melts. Geochim. Cosmochim. Acta. 60:4151-4160.

Métrich N., and Wallace P.J., 2008. Volatile abundances in basaltic magmas and their degassing paths tracked by melt inclusions. Rev. Mineral. Geochem. 69: 363–402.

Milia, A. and Torrente, M.M., 2007. The influence of paleogeographic setting and crustal subsidence on the architecture of ignimbrites in the Bay of Naples. Earth Planet Sci. Lett., 263, p. 192-193.

Moore G., 2008. Interpreting H2O and CO2 contents in melt inclusions: constraints from solubility experiments and modeling. Rev. Mineral. Geochem. 69:333-361.

Morhange, C., Marriner, N., Laborel, J., Todesco, M., and Oberlin, C., 2006, Rapid sea-level movements and noneruptive crustal deformations in the Phlegrean Fields caldera, Italy: Geology, v. 34 pp. 93-96 doi: 10.1130/G21894.1.

Mutchler S. R., Fedele L., and Bodnar R. J. (2007) AMS a new software package for reduction of Laser Ablation ICPMS data. ECROFI XIX.

Natale M., Nunziata C. and Panza G.F., 2005. Average shear wave velocity models of the crustal structure at Mt Vesuvius, Phys. Earth Planet. Inter. 152, pp. 7–21.

Newman, S., Lowenstern, J.B., 2002. VolatileCalc: a silicate melt-H2O-CO2 solution model written in Visual Basic for Excel: Computers and Geosciences vol. 28 no. 5, pp. 597-604.

Nunziata C., Natale M., Luongo G. and Panza G.F., 2006. Magma reservoir at Mt. Vesuvius: size of the hot, partially molten, crust material detected deeper than 8 km, Earth Planet. Sci. Lett. 242, pp. 51–57.

Orsi, G., D'Antonio, M., de Vita, S. and Gallo, G., 1992. The Neapolitan Yellow Tuff, a large-magnitude trachytic phreatoplinian eruption: eruptive dynamics, magma withdrawal and caldera collapse. J. Volcanol. Geotherm. Res. 53, pp. 275–287.

Orsi G., Civetta L., D'Antonio M., Di Girolamo P. and Piochi M., 1995. Step-filling and development of a three-layers magma chamber: the Neapolitan Yellow Tuff case history. J. Volcanol. Geotherm. Res., 67: 291-312.

Orsi G., de Vita S. and Di Vito M., 1996. The restless, resurgent Campi Flegrei nested caldera (Italy): constraints on its evolution and configuration. J. Volcanol. Geotherm. Res., 74: 179-214.

Orsi, G., Civetta, L., Del Daudio, C., de Vita, S., Di Vito, M.A., Isaia, R., Petrazzuoli, S.M., Ricciardi, G., Ricco, C., 1999. Short-term ground deformations and seismicity in the nested Campi Flegrei caldera (Italy): an example of active blockresurgence in a densely populated area. J. Volcanol. Geotherm. Res. 91, 415–451.

Pappalardo L., Civetta, L., D'Antonio, M., Deino, A., Di Vito, M., Orsi, G., Carandente, A., de Vita, S., Isaia, R. and Piochi, M.,, 1999 Chemical and Sr-isotopical evolution of the Phlegrean magmatic system before the Campanian Ignimbrite and the Neapolitan Yellow Tuff eruptions. J. Volcanol. Geotherm Res., vol.91, no.2-4, pp.141-166.

Parascandola A (1947) I fenomeni bradisismici del Serapeo di Pozzuoli. Genovese, Napoli.

Paterne M., Guichard F., 1993. Triggering of volcanic pulses in the Campanian area, south Italy, by periodic deep magma influx. J. Geophys. Res. 98: 1861-1873.

Peccerillo, A., 1999. Multiple mantle metasomatism in centralsouthern Italy: Geochemical e!ects, timing and geodynamic implications. Geology 27: 315-318.

Petrosino, P., Alberico, I., Caiazzo, S., Dal Piaz, A., Lire, L., and Scandone, R., 2004. Volcanic risk and evolution of the territorial system in the volcanic areas of Campania. Acta Vulcanol., vol.16, no.1-2, p. 163-178.

Piochi M., Mastrolorenzo G. and Pappalardo L., 2005. Magma ascent and eruptive processes from textural and compositional features of Monte Nuovo pyroclastic products, Campi Flegrei, Italy, *Bulletin of Volcanology* 67, pp. 663–678.

Poli S., Chiesa S., Gillot P.Y., Gregnanin A., Guichard F., Stella R., 1987. Major and trace element variation versus time in the volcanic products of Ischia (Gulf of Naples, Italy): Evidences of successive magmatic cycles. Contrib. Mineral. Petrol. 95: 322-333.

Raia F., Webster J. D. and De Vivo B., 2000. Pre-eruptive volatile contents of Vesuvius magmas: constrains on eruptive history and behavior. I - the medieval and modern interplinian activities. Eur. J. Mineral., 12: 179 – 193.

Roach, A., 2005. The evolution of silicic magmatism in the post-caldera volcanism of the Phlegrean fields, Italy. PhD thesis, Brown University.

Roedder E., (1979). Origin and significance of magmatic inclusions (In English with French and English abstracts). Bulletin de Mineralogie, 102, 467-510.

Rolandi G., Bellucci F., Heizler M.T., Belkin H.E. and De Vivo B., 2003. Tectonic controls on the genesis of ignimbrites from the Campanian Volcanic Zone, southern Italy. Mineralogy and Petrology, 79: 3 - 31.

Rosi M. and Sbrana A., 1987. Phlegrean Fields. CNR, Quaderni de "La Ricerca Scientifica", 114: 1-175.

Rosi M., Sbrana A., Vezzoli L., 1988. Stratigrafia delle isole di Procida e Vivara. Boll. GNV 4: 500-525.

Saito, G., K. Kazahaya, H. Shinohara, J. A. Stimac and Y. Kawanabe, 2001. Variation of volatile concentration in a magma system of Satsuma-Iwojima volcano deduced from melt inclusion analyses, J. Volcanol. Geotherm. Res. 108, 11-31.

Scandone R., Bellucci F., Lirer L. and Rolandi G., 1991. The structure of the Campanian Plain and the activity of the Neapolitan volcanoes (Italy). J. Volc. Geotherm. Res., 48: 1-31.

Schiano, P., 2003. Primitive mantle magmas recorded as silicate melt inclusions in igneous minerals. Earth-Sci. Rev. 63, 121–144.

Signorelli, S., Vaggelli, G., Romano, C., Carroll, M.R., 2001. Volatile element zonation in Campanian Ignimbrite magmas (Phlegrean Fields, Italy): evidence from the study of glass inclusions and matrix glasses. Contrib. Mineral. Petrol. 140, 543-553.

Sobolev, A.V., Shimizu, N., 1993. Ultradepleted primary melt included in olivine from the Mid-Atlantic Ridge. Nature 363, 151– 154.

Sobolev A.V., 1996. Melt inclusions in minerals as a source of principle petrological information. Petrology, 4, 209-220.

Spilliaert N., Allard P., Métrich N., Sobolev A., 2006. Melt inclusion record of the conditions of ascent, degassing and extrusion of volatile-rich alkali basalt during the powerful 2002 flank eruption of Mount Etna (Italy). J Geophys Res 111:B04203, doi: 10.1029/2005/JB003934.

Student, J.J., Bodnar, R.J., 2004. Silicate melt inclusions in porphyry copper deposits: identification and homogenization behavior. Can. Mineral. 42, 1563–1600.

Thomas JB & Bodnar RJ, 2002. A technique for mounting and polishing melt inclusions in small (<1 mm) crystals. American Mineralogist, 87: 1505-1508.

Thompson, R.N., 1982. Magmatism of the British Tertiary Volcanic Province. Scott. J. Geol. 18:49-107.

Tonarini S., Leeman W.P., Civetta L., D'Antonio M., Ferrara G., Necco A., 2004. B/Nb and $\delta^{11}B$ systematics in the Phlegrean Volcanic District Italy. Journal of Volcanology and Geothermal Research 133: 123-139.

Troise C., De Natale G., Pingue F., Obrizzo F., De Martino P., Tammaro U., and Boschi E. (2007) Renewed ground uplift at Campi Flegrei caldera (Italy): New insight on magmatic processes and forecast. Geophys. Res. Lett. 34, L03301. doi:10.1029/2006GL02854.

Turco E., Pierantoni P.P., Santarelli G., Schettino A., 2006. The Pleistocene extension of the Campanian Plain; morphotectonic analysis, kinematic model and implications for volcanism. In De Vivo B. "Volcanism in the Campania Plain: Vesuvius, Campi Flegrei and Ignimbrites" Elsevier Sciences B.V., pp. 58.

Wade J.A., Plank T., Melson W.G., Soto G.J., Hauri A.H., 2006. Volatile content of magmas from Arenal volcano, Costa Rica. J. Volcanol. Geotherm. Res. 157:94-120.

Wallace, P.J., A.T. Anderson, and A.M. Davis, 1999, Gradients in H2O, CO2 and exsolved gas in a large-volume silicic magma systems: interpreting the record preserved in melt inclusions from the Bishop Tuff, J. Geophys. Res. 104, 20097-20122.

Webster J.D., De Vivo B. and Tappen C., 2003 Volatiles, magmatic degassing and eruptions of Mt.Somma-Vesuvius: constraints from silicate melt incusions, Cl and $H_2O$ solubility experiments and modeling. In De Vivo B. and Bodnar R.J. "Melt inclusions in volcanic systems", Elsevier Sciences B.V., pp. 207-226.

Webster J. D., Raia F., De Vivo B. and Rolandi G., 2001. The behaviour of chlorine and sulfur during differentiation of the Mt. Somma-Vesuvius magmatic system. Mineralogy and Petrology, 73: 177-200.

Webster J. D., Raia F., Tappen C. and De Vivo B., 2003. Pre-eruptive geochemistry of the ignimbrite-forming magmas of the Campanian Volcanic Zone, Southern Italy, determined from silicate melt inclusions. Mineralogy and Petrology, 79: 99 – 125.

Webster J. D., Sintoni M. F. and De Vivo B., 2009. The partitioning behavior of Cl, S, and $H_2O$ in aqueous vapor- ± hypersaline-liquid saturated phonolitic and trachytic melts at 200 Mpa. Chemical Geology, 263, 19-36. doi:10.1016/j.chemgeo.2008.10.017.

Wohletz K., Orsi G., de Vita S., 1995. Eruptive mechanisms of the Neapolitan Yellow Tuff interpreted from stratigraphic, chemical, and granulometric data. J. Volcanol. Geotherm. Res. 67: 263-290.

Zollo A., Judenherc S., Auger E., D'Auria L., Virieux J., Capuano P., Chiarabba C., de Franco R., Makris J., Michelini A. and Musacchio G., 2003. Evidence for the buried rim of Campi Flegrei caldera from 3-d active seismic imaging. Geoph. Res. Lett., 30, 19: 2002, doi:10.1029/2003GL018173.

Zollo A., Maercklin N., Vassallo M., Dello Iacono D., Virieux J., and Gasparini P., 2008. Seismic reflections reveal a massive melt layer feeding Campi Flegrei caldera. Geophysical Research Letters, 35, L12306, doi:10.1029/2008GL034242.

Table 1. Summary of the eruptive events at Campi Flegrei <12 ka (From De Vito et al., 1999), plus the Solchiaro and the NYT. In orange are units collected for the PhD project.

| UNIT | AGE ka | STYLE | EPOCH |
|---|---|---|---|
| Solchiaro Volcano | 14.1-19.6 | phreatomagmatic to magmatic | before 12ka |
| Neapolitan Yellow Tuff | 15 | phreatomagmatic to magmatic | |
| Torre Cappella volcano | 12÷8.6 | phreatomagmatic explosions | |
| Bellavista volcano | 12÷8.6 | phreatomagmatic explosions | |
| Bacoli volcano | <12 | phreatomagmatic explosions | |
| Portomiseno volcano | <12 | phreatomagmatic explosions | |
| Capo Miseno volcano | <12 | phreatomagmatic explosions | |
| Contrada Murera volcano | 12÷8.6 | x | |
| Mofete volcano | 12÷10.7 | phreatomagmatic explosions | |
| Gauro Volcano | 12÷10.7 | mostly phreatomagmatic explosions | |
| Archiaverno volcano | 10.7 | mostly phreatomagmatic explosions | |
| Rione Terra volcano | 12÷10 | phreatomagmatic explosions | |
| La Pietra volcano | 12÷10 | phreatomagmatic explosions | |
| Santa Teresa volcano | 12÷10.3 | mostly phreatomagmatic explosions | |
| LP-NYT | 11.1 | x | |
| La Pigna 1 Tephra | 11.1 | phreatomagmatic explosions | |
| La Pigna 2 Tephra | 11.1÷9.5 | magmatic/hydromagmatic explosions | |
| Minopoli 1 Tephra | 11.1÷10.3 | strombolian with subordinate phreatomagmatic explosions | |
| Paradiso Tephra | 11.1÷9.5 | phreatomagmatic with subordinate magmatic explosion | |
| Soccavo 1 Tephra | 10.3 | mostly phreatomagmatic explosions | |
| PP-S1 1÷4 | 10.3 | x | I |
| Gaiola Tephra | 10.3 | magmatic and hydromagmatic explosions | |
| Pomici Principali Tephra | 10.3 | phreatomamatic and magmatic explosion | |
| Soccavo 2 Tephra | 10.3÷9.5 | phreatomamatic and magmatic explosion | |
| Soccavo 3 Tephra | 10.3÷9.5 | phreatomagmatic explosions | |
| Soccavo 4 Tephra | 10.3÷9.5 | phreatomagmatic with subordinate magmatic explosion | |
| Minopoli 2 Tephra | 10.3÷9.5 | magmatic with subordinate phreatomagmatic explosion | |
| S5-M2 1÷4 | 10.3÷9.5 | x | |
| Soccavo 5 Tephra | 10.3÷9.5 | magmatic and phreatomagmatic explosions | |
| Banco di Nisida Volcano | 10.3÷9.5 | x | |
| Nisida Tephra | 10.3÷9.5 | mostly phreatomagmatic explosions | |
| Pisani 1 | 10.3÷9.5 | magmatic with subordinate phreatomagmatic explosion | |
| Pisani 2 | 10.3÷9.5 | phreatomamatic and magmatic explosion | |
| Montagna Spaccata Tephra | 10.3÷9.5 | strombolian with subordinate phreatomagmatic explosions | |
| Fondo Riccio Volcano | 10.3÷9.5 | strombolian explosions | |
| Concola volcano | 10.3÷9.5 | strombolian explosions | |
| Pignatello 1 Tephra | 10.3÷9.5 | phreatomamatic and magmatic explosion | |
| Pisani 3 | 9.5 | phreatomagmatic with subordinate magmatic explosion | |
| Casale Tephra | 9.5÷8.6 | phreatomamatic and magmatic explosion | |
| Fondi di Baia Tephra | 8.6 | phreatomagmatic with subordinate magmatic explosion | |
| Sartania I Tephra | 8.6 | phreatomagmatic explosions | |
| Costa San Domenico Tephra | 8.6÷8.2 | mostly phreatomagmatic explosions | II |
| Pigna San Nicola Tephra | 8.6÷8.2 | phreatomamatic and magmatic explosion | |
| Sartania 2 Tephra | 8.6÷8.2 | phreatomamatic and magmatic explosion | |
| San Martino Tephra | 8.2 | phreatomamatic and magmatic explosion | |
| Agnano 1 Tephra | 4.8 | phreatomamatic and magmatic explosion | |
| Averno 1 Tephra | 4.5 | mostly phreatomagmatic explosions | |
| Agnano 2 Tephra | 4.5÷4.4 | mostly phreatomagmatic explosions | |
| Monte Spina Lavas | 4.5÷4.4 | lava effusion | |
| Agnano 3 Tephra | 4.5÷4.4 | phreatomagmatic with subordinate magmatic explosion | |
| Cigliano Tephra | 4.5÷4.4 | phreatomagmatic with subordinate magmatic explosion | |
| Pignatello 2 Tephra | 4.5÷4.4 | phreatomagmatic with subordinate magmatic explosion | |
| Monte Sant'Angelo Tephra | 4.4 | phreatomagmatic with subordinate magmatic explosion | |
| Paleoastroni 1 Tephra | 4.4÷4.2 | phreatomagmatic with subordinate magmatic explosion | |
| Paleoastroni 2 Tephra | 4.2 | phreatomagmatic with subordinate magmatic explosion | |
| Agnano-Monte Spina Tephra | 4.1 | phreatomagmatic with subordinate magmatic explosion | III |
| Monte Olibano Lavas | 4.1÷3.8 | lava effusion | |
| Accademia Lavas | 4.1÷3.8 | lava effusion | |
| Solfatara Tephra | 4.1÷3.8 | phreatomagmatic with subordinate magmatic explosion | |
| Averno 2 Tephra | 4.1÷3.8 | phreatomamatic and magmatic explosion | |
| Caprara Lavas | 4.1÷3.8 | lava effusion | |
| Astroni 1 Tephra | 4.1÷3.8 | phreatomagmatic with subordinate magmatic explosion | |
| Astroni 2 Tephra | 4.1÷3.8 | phreatomagmatic with subordinate magmatic explosion | |
| Astroni 3 Tephra | 3.8 | phreatomagmatic with subordinate magmatic explosion | |
| Fossa Lupara Tephra | 3.8 | phreatomagmatic and strombolian type explosions | |
| Monte Nuovo Tephra | 1538 AD | phreatomagmatic and strombolian type explosions | |

Tab. 2. Petrography of representative MI from RESC2, RESC3, RESC4, RESC5 sample. All MI are hosted in olivine.

| Inclusion ID | shape | max section size (μm2) | Bubbles | associated crystal | zoning Fe/Mg |
|---|---|---|---|---|---|
| RESC2-O26-M1 | ellipsoidal | 3.77E+03 | 1 | chromite | none |
| RESC2-O26-M2 | spherical | 7.07E+02 | none | chromite | none |
| RESC2-O26-M3 | ellipsoidal | 1.34E+04 | 1 | none | none |
| RESC2-O26-M4 | irregular | 5.00E+04 | 4 | none | none |
| RESC2-O52-MA | negative crystal | 2.36E+04 | none | chromite | none |
| RESC3-O16-MA | negative crystal | 1.37E+03 | none | chromite | yes oscillatory |
| RESC3-O16-MB | negative crystal | 1.96E+03 | 1 | chromite | yes oscillatory |
| RESC3-O22-MA | spherical | 5.03E+03 | none | none | none |
| RESC3-O22-MC | ellipsoidal | 6.28E+03 | 1 | chromite | none |
| RESC3-O23-MA | irregular | 7.85E+03 | none | none | yes reverse |
| RESC3-O23-MC | irregular | 7.85E+03 | 1 | none | yes reverse |
| RESC4-O2-MA | ellipsoidal | 1.88E+03 | none | none | yes oscillatory |
| RESC4-O3-MA | spherical | 4.15E+02 | none | chromite | yes oscillatory |
| RESC4-O7-MA | ellipsoidal | 3.93E+03 | none | none | none |
| RESC5-O5-MA | ellipsoidal | 1.37E+03 | none | none | yes, reverse |
| RESC5-O8-MA | ellipsoidal | 2.20E+03 | 1 | chromite | yes, normal |
| RESC5-O8-MB | spherical | 1.13E+04 | 1 | diopside, chromite | yes, normal |
| RESC5-O13-MA | negative crystal | 6.05E+03 | 1 | chromite | yes, oscillatory |
| RESC5-O13-MC | negative crystal | 8.80E+03 | 1 | none | yes, oscillatory |
| RESC5-O13-MD | negative crystal | 1.26E+04 | 1 | none | yes, oscillatory |

Tab. 3. EPMA representative analysis of olivine from RESC3, RESC4, RESC5.

| | wt% | | | | | | mole% | | | |
|---|---|---|---|---|---|---|---|---|---|---|
| | $SiO_2$ | FeO | MnO | MgO | CaO | Total | %Fo | %Fa | %Mn-Ol | %Ca-Ol |
| RESC3-O16-H1-core | 39.59 | 11.08 | 0.24 | 43.58 | 0.32 | 95.15 | 86.89 | 12.39 | 0.27 | 0.46 |
| RESC3-O16-H2-rim | 37.19 | 16.86 | 0.30 | 37.12 | 0.28 | 92.53 | 79.06 | 20.14 | 0.36 | 0.43 |
| RESC3-O22-H1-core | 39.57 | 12.11 | 0.25 | 43.14 | 0.37 | 95.59 | 85.71 | 13.49 | 0.28 | 0.52 |
| RESC3-O23-H2-core | 38.88 | 15.88 | 0.27 | 39.55 | 0.28 | 95.11 | 81.02 | 18.25 | 0.32 | 0.41 |
| RESC3-O23-H4-rim | 39.54 | 12.00 | 0.16 | 42.60 | 0.34 | 95.02 | 85.76 | 13.55 | 0.18 | 0.50 |
| RESC4-O7-H1-core | 40.62 | 13.87 | 0.19 | 43.69 | 0.34 | 98.87 | 84.30 | 15.02 | 0.21 | 0.47 |
| RESC4-O2-H1-core | 40.50 | 14.91 | 0.26 | 42.73 | 0.31 | 98.81 | 83.03 | 16.25 | 0.29 | 0.43 |
| RESC4-O3-H1-core | 41.58 | 10.97 | 0.19 | 45.95 | 0.34 | 99.18 | 87.60 | 11.73 | 0.21 | 0.46 |
| RESC4-O3-H3-rim | 41.11 | 12.42 | 0.18 | 44.64 | 0.34 | 98.79 | 85.92 | 13.41 | 0.20 | 0.47 |
| RESC5-O5-H1-core | 40.88 | 11.82 | 0.18 | 45.34 | 0.32 | 98.65 | 86.68 | 12.68 | 0.20 | 0.44 |
| RESC5-O5-H3-rim | 41.57 | 10.06 | 0.11 | 46.19 | 0.26 | 98.31 | 88.68 | 10.84 | 0.12 | 0.36 |
| RESC5-O8-H1-core | 41.71 | 9.06 | 0.19 | 47.28 | 0.34 | 98.65 | 89.68 | 9.65 | 0.21 | 0.46 |
| RESC5-O8-H3-rim | 41.42 | 11.89 | 0.15 | 45.67 | 0.29 | 99.52 | 86.76 | 12.67 | 0.17 | 0.40 |

Tab. 4. XRF analysis from bulk rock of this study. Fo mol% was calculated using petrolog software (Danyushevsky) using Ford et al. (2003) equilibrium equation and assuming NNO buffer and the ratio $Fe^{2+}/Fe^{3+}$ was determined using Borisov and Shapkin (1990) equation.

| Sample | RE SC 2-a | RE SC 2-b | RE SC 3-a | RE SC 3-b | RE SC 4-a | RE SC 4-b | RE SC 5 | |
|---|---|---|---|---|---|---|---|---|
| $SiO_2$ | 49.31 | 47.73 | 48.85 | 48.73 | 49.44 | 49.78 | 48.64 | |
| $TiO_2$ | 1.23 | 1.3 | 1.26 | 1.28 | 1.22 | 1.23 | 1.27 | |
| $Al_2O_3$ | 16.96 | 18.22 | 16.9 | 17.38 | 17.49 | 17.88 | 17.09 | |
| $Fe_2O_3$ | 1.59 | 1.49 | 1.53 | 1.4 | 1.69 | 1.53 | 1.55 | |
| FeO | 7.36 | 7.18 | 7.31 | 6.94 | 7.02 | 6.95 | 7.23 | |
| MnO | 0.13 | 0.15 | 0.13 | 0.14 | 0.14 | 0.15 | 0.13 | wt% |
| MgO | 6.64 | 6.94 | 6.88 | 7.02 | 5.62 | 5.69 | 6.73 | |
| CaO | 10.5 | 10.69 | 11.2 | 11.24 | 9.99 | 9.87 | 11.2 | |
| $Na_2O$ | 3.03 | 3.07 | 2.79 | 2.86 | 3.39 | 2.96 | 2.96 | |
| $K_2O$ | 2.8 | 2.78 | 2.68 | 2.57 | 3.44 | 3.39 | 2.74 | |
| $P_2O_5$ | 0.42 | 0.44 | 0.45 | 0.45 | 0.56 | 0.56 | 0.46 | |
| $Cr_2O_3$ | 0.02 | 0 | 0.02 | 0 | 0.01 | 0 | 0.02 | |
| Fo | 84.52 | 85.77 | 85.07 | 86.09 | 83.1 | 83.17 | 85.02 | mol% |
| Mg# | 61.65 | 63.25 | 62.65 | 64.32 | 58.79 | 59.32 | 62.35 | |
| Be | 2 | 0 | 2 | 0 | 2 | 0 | 2 | |
| B | 0 | 0 | 0 | 0 | 0 | 0 | 0 | |
| V | 191 | 180 | 207.5 | 186 | 204 | 179 | 209 | |
| Cr | 0 | 129 | 0 | 108 | 0 | 60.5 | 0 | |
| Co | 31.3 | 30 | 33.1 | 30 | 28.4 | 26 | 33.4 | |
| Ni | 88 | 64.5 | 79 | 65 | 56 | 43 | 77 | |
| Rb | 88.7 | 89 | 84 | 80 | 103.6 | 102 | 86.9 | |
| Sr | 653.8 | 576 | 688.3 | 604 | 761.6 | 656 | 719.3 | |
| Y | 26.5 | 26.4 | 24.55 | 23.9 | 25.4 | 24.1 | 25.5 | |
| Zr | 139.7 | 156 | 123.1 | 127 | 140.6 | 144 | 122.9 | |
| Nb | 19.1 | 18.4 | 17.5 | 16.6 | 20.1 | 18.5 | 17.6 | |
| Cs | 5.1 | 5.8 | 3.8 | 3.8 | 4.8 | 4.9 | 4.1 | |
| Ba | 682 | 780 | 790.45 | 818 | 890.3 | 930 | 814.8 | |
| La | 31.9 | 29.7 | 26.65 | 24.1 | 37.2 | 32.9 | 27 | |
| Ce | 66.7 | 60.4 | 57.25 | 50.7 | 77.6 | 68 | 59.8 | ppm |
| Pr | 7.85 | 7.02 | 6.96 | 6 | 9.18 | 7.83 | 7.09 | |
| Nd | 31.9 | 28.8 | 28.65 | 25.3 | 37.8 | 31.7 | 28.9 | |
| Sm | 6.3 | 5.98 | 6.45 | 5.59 | 7.5 | 6.43 | 6.6 | |
| Eu | 1.84 | 1.77 | 1.9 | 1.76 | 2.13 | 1.95 | 1.9 | |
| Gd | 5.98 | 5.58 | 5.86 | 5.36 | 6.51 | 5.89 | 5.13 | |
| Tb | 0.94 | 0.87 | 0.88 | 0.83 | 1.01 | 0.87 | 0.94 | |
| Dy | 5.07 | 4.88 | 4.59 | 4.67 | 5.17 | 4.63 | 4.88 | |
| Yb | 2.39 | 2.12 | 2.23 | 2 | 2.07 | 2.02 | 2.22 | |
| Lu | 0.32 | 0.33 | 0.32 | 0.3 | 0.33 | 0.3 | 0.31 | |
| Hf | 3.2 | 3.6 | 3.35 | 3 | 3.5 | 3.4 | 3 | |
| Ta | 1 | 1.14 | 1.05 | 1.08 | 1.2 | 1.21 | 0.9 | |
| Pb | 48.4 | 11 | 8.95 | 10 | 11.4 | 12 | 8.3 | |
| Th | 8 | 7.22 | 5.4 | 5.33 | 6.7 | 7.53 | 5.1 | |
| U | 2.1 | 2.06 | 1.65 | 1.58 | 2.1 | 2.22 | 1.4 | |

Tab.5. Major/trace element and volatile of characteristic MI (corrected with petrolog software by Danyushevsky of Solchiaro eruption. $X_{ol}$ = percentage of olivine crystallized after entrapment of the melt; FeO and $Fe_2O_3$ are calculated based on Borisov and Shapkin 1990 equation and assuming NNO buffer; Mg# = 100*Mg/(Mg+$Fe^{2+}$); major elements and $H_2O$ are in wt% and trace elements are in ppm.

| | RESC2-O26.MI1 | RESC2-O26.MI3 | RESC2-O52.MIA | RESC3-O22-MA | RESC3-O16-MA | RESC3-O23-MC | RESC4-O7-MA | RESC4-O3-MA | RESC4-O2-MA | RESC5-O5-MA | RESC5-O8-MC | RESC5-O13-MC |
|---|---|---|---|---|---|---|---|---|---|---|---|---|
| type | $K_2O$-lowest MI | High-Fo MI | Low-Fo MI | $K_2O$-lowest MI | High-Fo MI | Low-Fo MI | $K_2O$-lowest MI | High-Fo MI | Low-Fo MI | $K_2O$-lowest MI | High-Fo MI | Low-Fo MI |
| $SiO_2$ | 49.10 | 49.86 | 51.54 | 50.93 | 52.22 | 50.84 | 49.84 | 49.72 | 49.56 | 50.10 | 50.65 | 49.61 |
| $TiO_2$ | 0.63 | 1.30 | 1.07 | 0.38 | 1.20 | 1.33 | 1.45 | 1.80 | 1.20 | 1.31 | 1.19 | 1.20 |
| $Al_2O_3$ | 17.26 | 16.88 | 17.53 | 17.12 | 17.31 | 16.94 | 15.68 | 17.64 | 17.72 | 15.63 | 15.79 | 16.43 |
| $Fe_2O_3$ | 1.07 | 1.19 | 1.40 | 0.94 | 1.01 | 2.01 | 1.54 | 1.06 | 1.63 | 1.30 | 1.24 | 1.70 |
| FeO | 6.99 | 6.21 | 6.91 | 6.77 | 5.00 | 7.78 | 7.81 | 5.61 | 7.10 | 7.22 | 5.54 | 7.77 |
| MnO | 0.14 | 0.12 | 0.15 | 0.12 | 0.13 | 0.15 | 0.14 | 0.06 | 0.18 | 0.11 | 0.11 | 0.13 |
| MgO | 7.53 | 6.71 | 5.57 | 7.20 | 5.49 | 5.51 | 7.21 | 6.52 | 5.77 | 8.10 | 5.97 | 6.63 |
| CaO | 13.89 | 12.22 | 9.41 | 13.63 | 10.66 | 7.08 | 11.77 | 12.07 | 9.41 | 12.09 | 12.36 | 10.22 |
| $Na_2O$ | 1.94 | 2.56 | 2.73 | 2.20 | 2.57 | 2.91 | 2.65 | 2.33 | 2.56 | 2.52 | 2.26 | 2.23 |
| $K_2O$ | 1.18 | 2.47 | 3.11 | 0.51 | 3.86 | 4.66 | 1.57 | 2.74 | 4.17 | 1.22 | 4.20 | 3.58 |
| $P_2O_5$ | 0.23 | 0.47 | 0.47 | 0.18 | 0.47 | 0.80 | 0.32 | 0.45 | 0.71 | 0.30 | 0.60 | 0.48 |
| $Cr_2O_3$ | 0.1 | 0.0 | 0.1 | 0.03 | 0.08 | 0.00 | 0.03 | 0.02 | 0.00 | 0.11 | 0.09 | 0.03 |
| Fo | 86.25 | 86.64 | 82.45 | 85.71 | 86.9 | 81.03 | 84.30 | 87.60 | 83.04 | 86.79 | 86.76 | 83.42 |
| Mg# | 65.74 | 65.80 | 58.97 | 65.45 | 66.17 | 55.79 | 62.19 | 67.44 | 59.15 | 66.66 | 65.78 | 60.32 |
| $X_{ol}$ | 3.6 | 2.1 | 1.1 | 3.9 | 1.6 | 3.1 | 4.5 | 6.9 | 1.9 | 9.1 | 2.4 | 6.2 |
| Be | 7 | 8 | - | - | 3 | - | - | - | - | - | - | 2 |
| B | - | - | 18 | - | 13 | 17 | 6 | - | 15 | - | 28 | 18 |
| V | 186 | 184 | 145 | 210 | 166 | 238 | 185 | 256 | 207 | 222 | 240 | 191 |
| Cr | 114 | 174 | 80 | 149 | 117 | 15 | 104 | 96 | 19 | 297 | 144 | 55 |
| Co | 28 | 21 | 26 | 28 | 19 | 30 | 35 | - | 28 | - | 24 | 23 |
| Ni | 55 | 48 | 51 | 38 | 26 | 17 | 39 | - | 40 | - | 50 | 36 |
| Rb | 37 | 90 | 123 | 5 | 101 | 152 | 51 | 105 | 141 | 46 | 162 | 135 |
| Sr | 1262 | 451 | 535 | 1832 | 552 | 757 | 440 | 591 | 700 | 482 | 757 | 632 |
| Y | 16 | 16 | 16 | 18 | 16 | 21 | 20 | 17 | 16 | 23 | 24 | 16 |
| Zr | 33 | 98 | 96 | 7 | 108 | 129 | 94 | 103 | 109 | 119 | 170 | 107 |
| Nb | 6 | 15 | 19 | 1 | 22 | 23 | 10 | 15 | 20 | 11 | 29 | 16 |
| Cs | 8 | 8 | 5 | 1 | n.a. | 9 | 3 | n.a | 10 | n.a | 7 | 6 |
| Ba | 431 | 694 | 902 | 400 | 896 | 1361 | 431 | 929 | 1161 | 526 | 1512 | 1020 |
| La | 10 | 17 | 23 | 5 | 28 | 39 | 12 | 19 | 29 | 16 | 36 | 25 |
| Ce | 19 | 37 | 50 | 8 | 55 | 75 | 28 | 42 | 63 | 36 | 76 | 51 |
| Pr | 2 | 4 | 6 | 1 | 6 | 9 | 4 | 6 | 7 | 5 | 9 | 6 |
| Nd | 10 | 19 | 22 | 5 | 26 | 37 | 17 | 30 | 30 | 24 | 37 | 27 |
| Sm | 2.4 | 4.3 | 4.3 | 1.0 | 5.2 | 8.0 | 3.8 | 4.0 | 6.2 | 4.7 | 7.4 | 5.3 |
| Eu | 0.9 | 1.7 | 1.5 | 0.9 | 1.8 | 2.2 | 1.2 | 2.2 | 2.1 | 3.2 | 2.3 | 1.7 |
| Gd | 2.1 | 3.8 | 4.8 | 1.2 | 4.4 | 6.2 | 4.6 | 4.5 | 5.6 | 4.2 | 8.5 | 4.7 |
| Tb | 0.3 | 0.5 | 0.5 | 0.3 | 0.7 | 0.9 | 0.6 | - | 0.6 | 1.2 | 1.0 | 0.6 |
| Dy | 2.8 | 3.0 | 3.4 | 2.7 | 3.7 | 4.6 | 3.6 | 4.2 | 3.4 | - | 5.4 | 3.4 |
| Yb | 1.81 | 1.02 | 1.40 | 1.91 | 1.36 | 2.38 | 1.87 | n.a. | 1.43 | 3.91 | 2.48 | 1.67 |
| Lu | - | - | - | - | 0.39 | 0.72 | - | - | - | - | - | 0.43 |
| Hf | 1.21 | 1.80 | 2.84 | - | 2.41 | 3.14 | 2.56 | 3.53 | 2.57 | 1.60 | 4.94 | 2.77 |
| Ta | - | 0.68 | 0.79 | - | 0.94 | 1.19 | 0.56 | 0.52 | 0.96 | 0.44 | 1.43 | 0.65 |
| Pb | 5.2 | 11.1 | 13.1 | 1.9 | 12.8 | 18.1 | 6.9 | 16.7 | 16.0 | 9.7 | 20.9 | 14.8 |
| Th | 1.8 | 4.3 | 5.2 | 0.2 | 6.2 | 7.8 | 2.5 | 7.3 | 6.7 | 3.3 | 10.9 | 6.3 |
| U | - | - | 0.0 | 0.1 | 1.7 | 2.7 | 0.7 | 1.9 | 2.3 | 1.2 | 3.7 | 2.1 |
| $CO_2$ | 103 | 637 | 523 | 76 | 252 | 219 | 439 | 325 | 143 | 916 | 713 | 520 |
| $H_2O$ | 1.06 | 1.07 | 1.31 | 1.10 | 1.14 | 1.13 | 0.96 | 1.18 | 1.08 | 1.19 | 1.48 | 1.26 |
| F | 1079 | 980 | 1455 | 1293 | 897 | 1392 | 724 | 718 | 1227 | 603 | 1987 | 1659 |
| S | 283 | 1418 | 1189 | 34 | 829 | 1700 | 1297 | 1355 | 1415 | 1180 | 1769 | 1093 |
| Cl | 719 | 2719 | 2451 | 89 | 1310 | 2833 | 1286 | 2691 | 2611 | 1232 | 4076 | 1700 |

FIGURES AND CAPATIONs

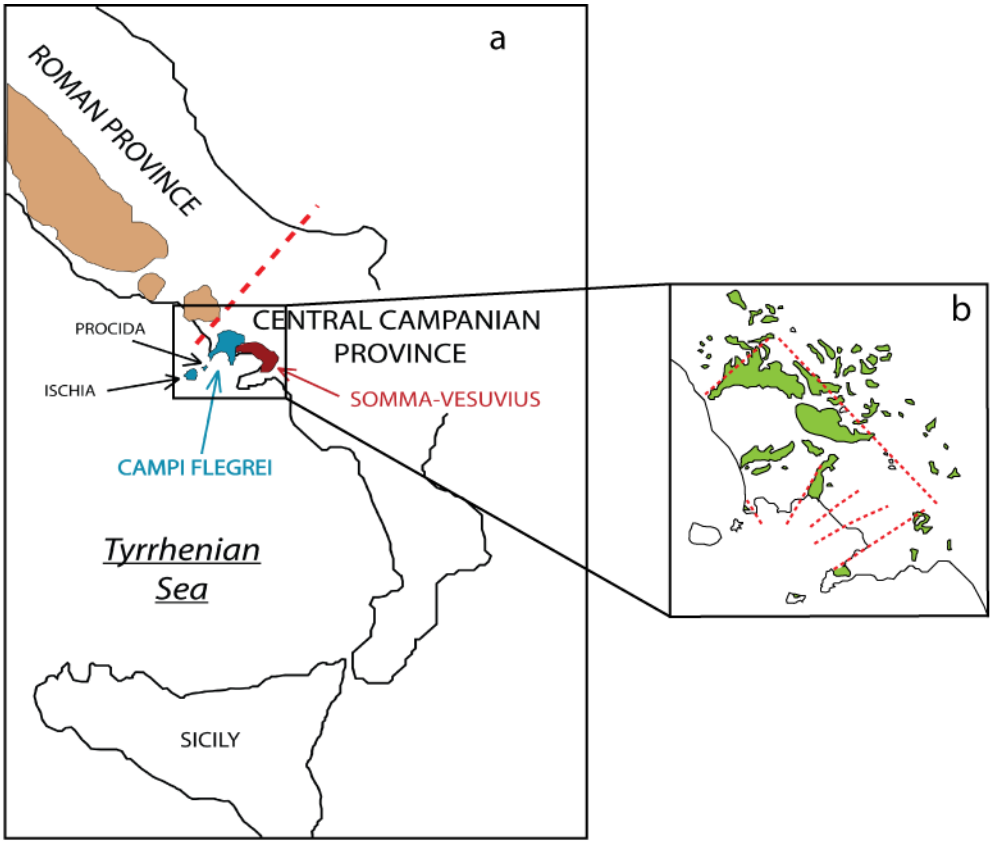


Fig. 1. a) Distribution of volcanism of the central-southern sector of Italy (after Tonarini et al., 2004). The red dashed line represents the Ortona-Roccamonfina structural line separating the Roman Province and the Central Campanian Province. b) Map of Campanian Ignimbrite outcrops (green areas) and the main tectonic structures in the Campanian Plain (red dotted lines) after De Vivo et al. (2001).

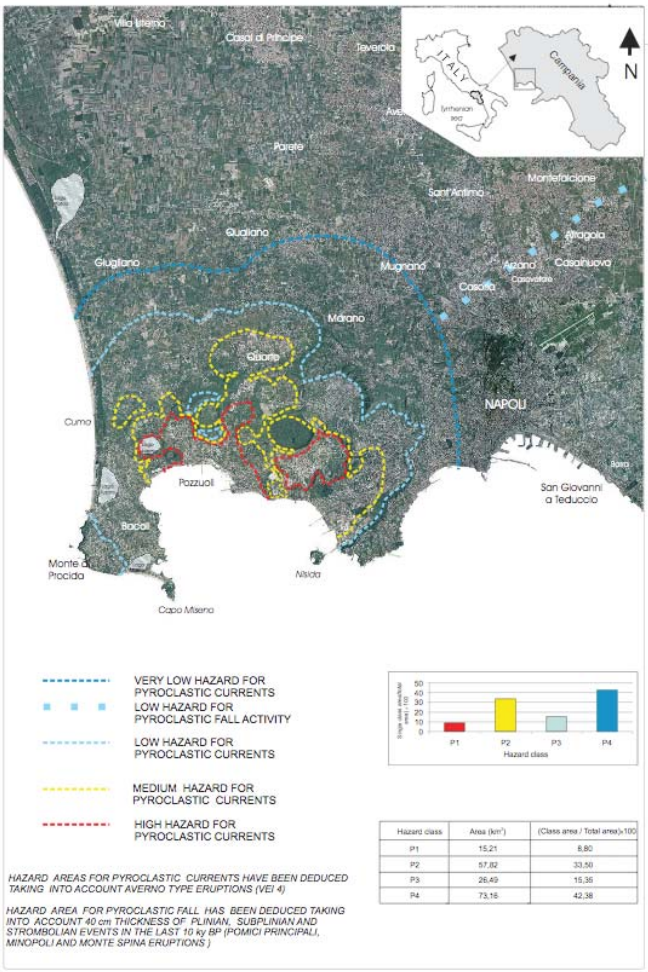


Fig. 2. Risk map showing the areas of potential hazards associated with pyroclastic flows and ash falls in the Campi Flegrei area. Note the large areas at risk from pyroclastic flows; the entire Campi Flegei area is at high risk from ash falls >40 cm thick (Modified from Petrosino et al., 2004)

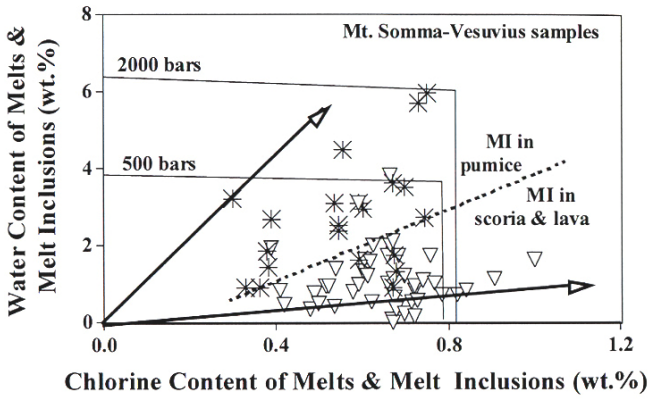


Fig. 3. Concentrations of $H_2O$ and Cl in Somma-Vesuvius magmas and $H_2O$ and Cl abundances of MI from Somma-Vesuvius distinguished according to eruptive style (From Webster et al., 2003).

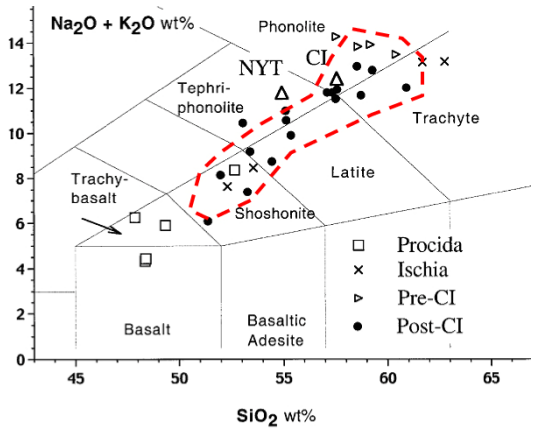


Fig. 4. Total alkali vs. silica classification diagram (TAS; Le Bas et al., 1986) for samples from Campi Flegrei. The red dotted line encompasses the range in compositions from volcanic rocks < 12 ka (After Tonarini et al., 2004).

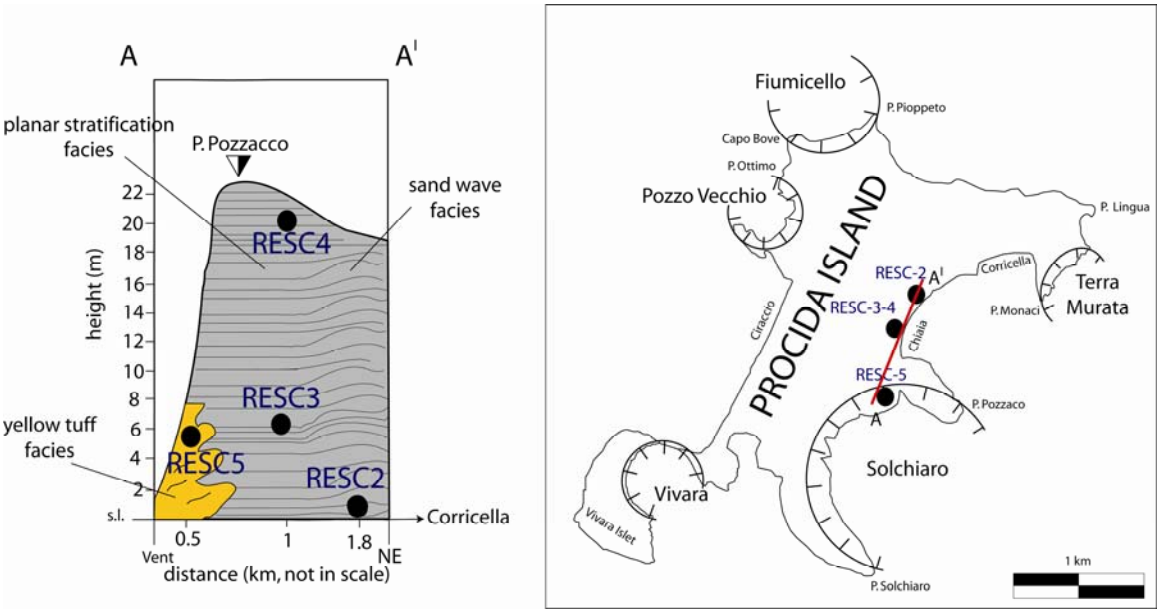


Fig. 5. Procida Island map showing volcanic vents recognized (De Astis et al., 2004) and the sample locations (right). On the left, is shown a simplified stratigraphic column reporting the chronostratigraphic relation among the collected samples.

Fig. 6. Outcrop of the Solchiaro eruption on Procida Island showing the sand wave facies at the cliff between Punta Pizzacco and Spiaggia della Corricella.

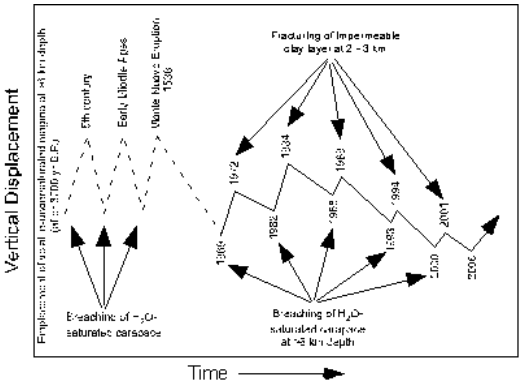


Fig. 7. Vertical ground displacement versus time in the vicinity of Pozzuoli, Italy from Bodnar et al. 2007. Note that both vertical displacement and time are schematic and only indicate the direction of ground movement at different times. [Modified from (De Natale et al., 2001; Dvorak and Mastrolorenzo, 1991;)].

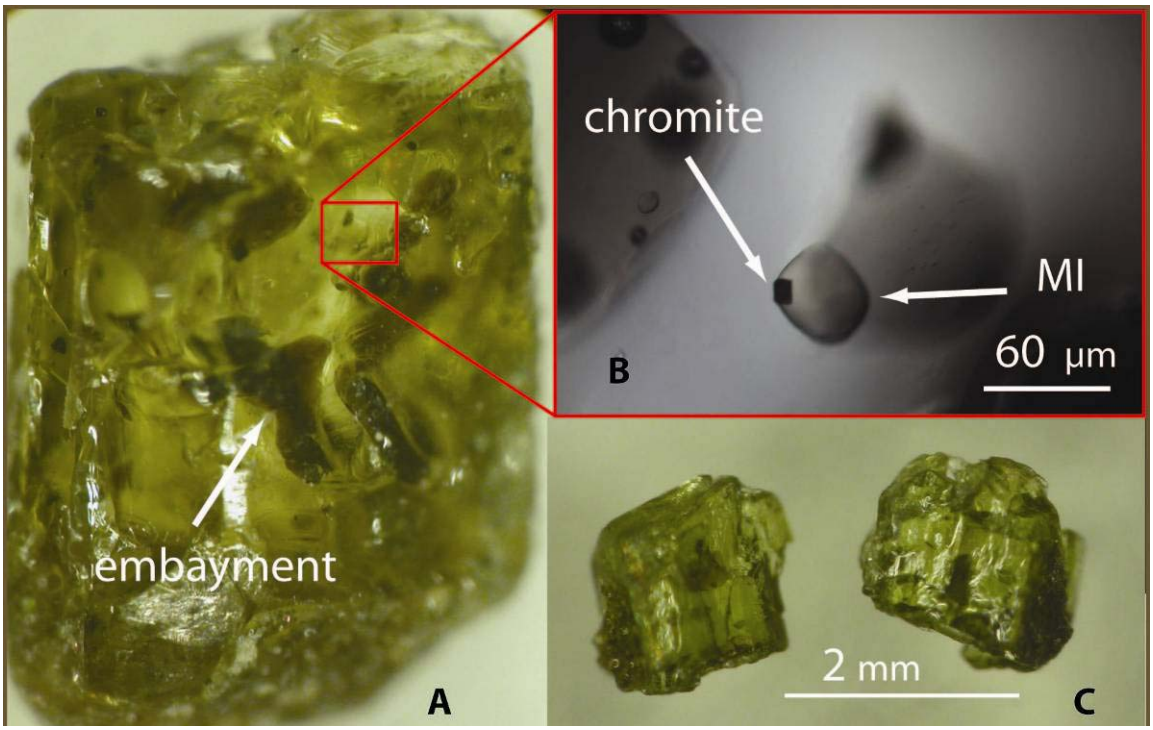


Fig. 8. Photos from RESC2 sample: A- 2.5 mm olivine phenocryst (O26) picked up from the sample and cleaned with ultrasound-waves (Picture took from a binocular microscope). The sample 25X magnified shows even with out polishing or oil immersion neat glass embayment (in brown) and MIs associated with

chromite crystal. B- Colorless MIs associated with chromite crystal but not bubble. C- Clinopyroxene phenocryst less than 2 mm in diameter into which is possible to observe brown glass.

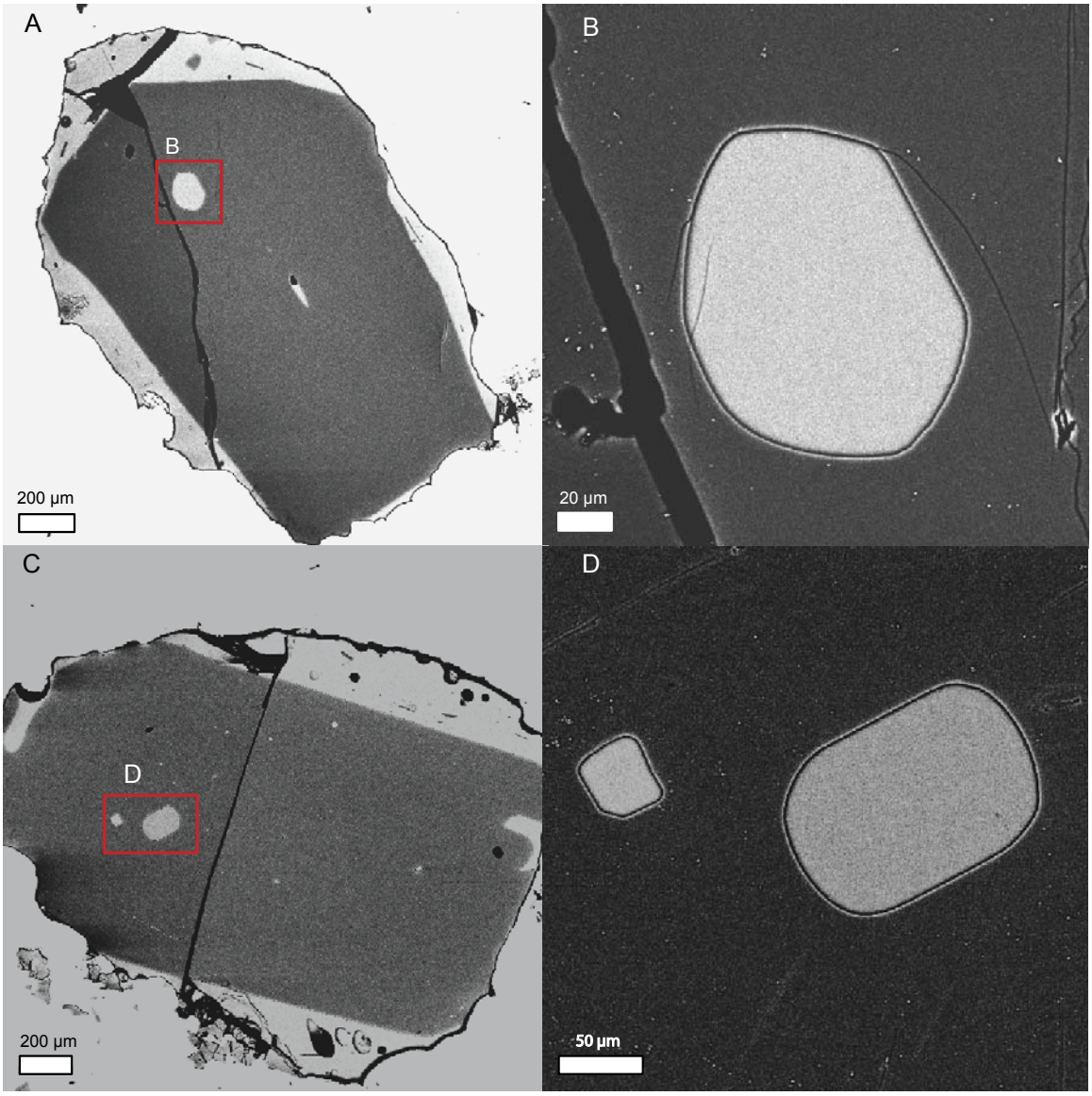


Fig. 9. Back-scattered electron images of olivine phenocrysts and MI from the Solchiaro eruption (RESC3 sample). A-C) Euhedral olivines containing MI, glass reentrants and poorly vesciculated glass rim; C-D) MIs showing faceted shape and homogeneous element distribution. Note the Fe-rich olivine rim at the melt-host interface that represents precipitation on the wall after MI entrapment (Kent, 2008).

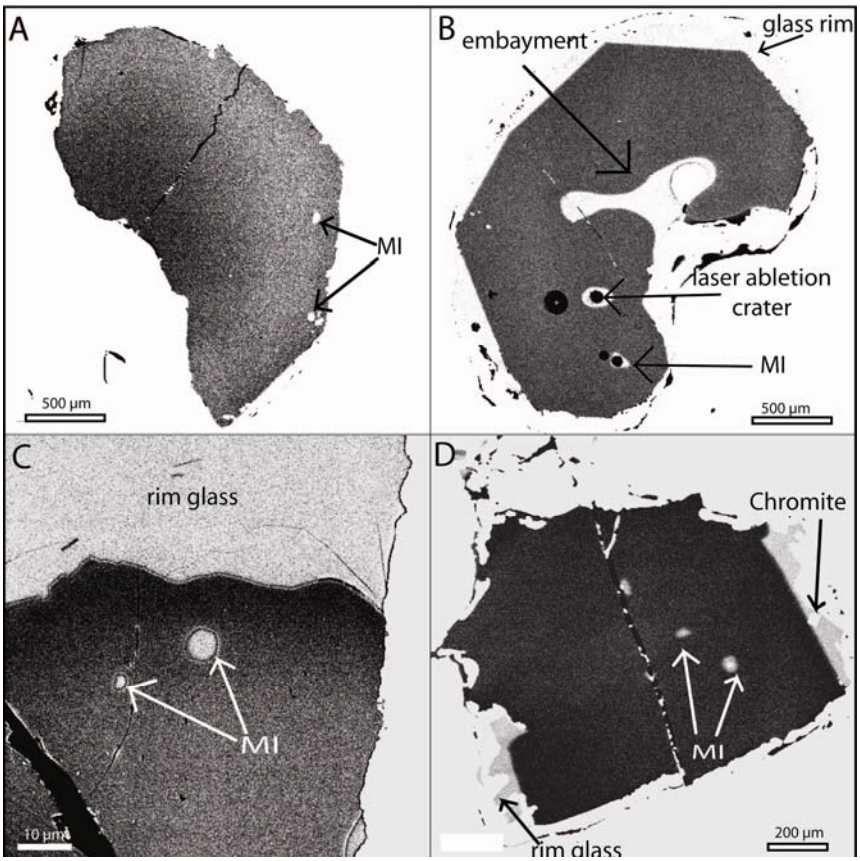


Fig. 10. Back-scattered electron images of olivine phenocrysts from RESC2 sample. A- O8 olivine is illustrated to note of the hollow shape (see text); B- O13 olivine showing embayment and characteristic hollow shape; C- O22 showing its strongly reverse zoning from $Fo_{82}$ on the core and $Fo_{86}$ ont the rim; D- O12 is also strongly reversed and at in contact with the rim is present a chromite phenocryst.

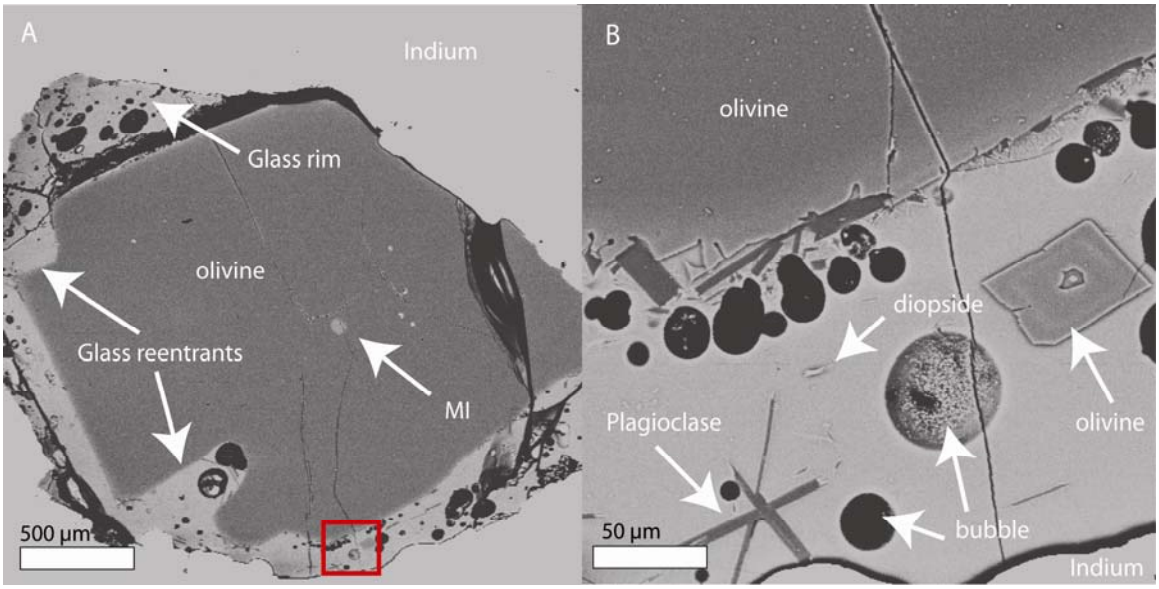


Fig.11. Olivine RESC3-O2 showing: A) glass rim, glass reentrants with bubbles and MI; B) microphenocrysts of plagioclase, diopside with tabular and dendritic shape, and olivine with oscillatory zoning and glass in the core. Note the bubbles are never in direct contact with olivine but preferentially with dendritic plagioclase.

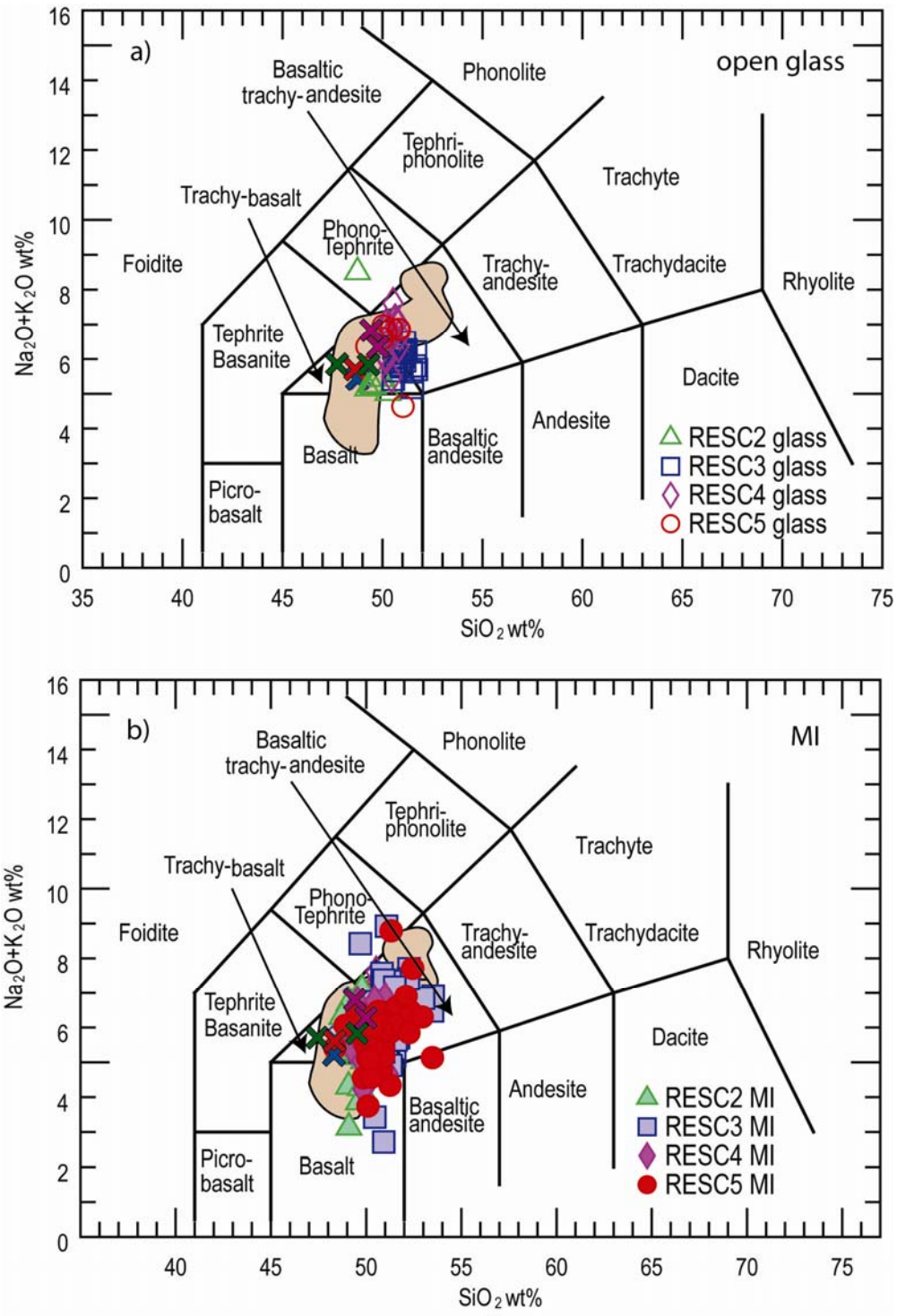


Fig. 12. a) Classification based on the TAS diagram from Le Bas et al. (1986) of open glasss (open symbols) and bulk rocks from this study (crosses: green=RESC2, blue=RESC3, purple=RESC4, red=RESC5), also reported are bulk rock from literature (pink area; data from Di Girolamo et al., 1984; D'Antonio et al. 1999; De Astis et al., 2004). b) corrected MI (filled symbols), bulk rock from this study and literature.

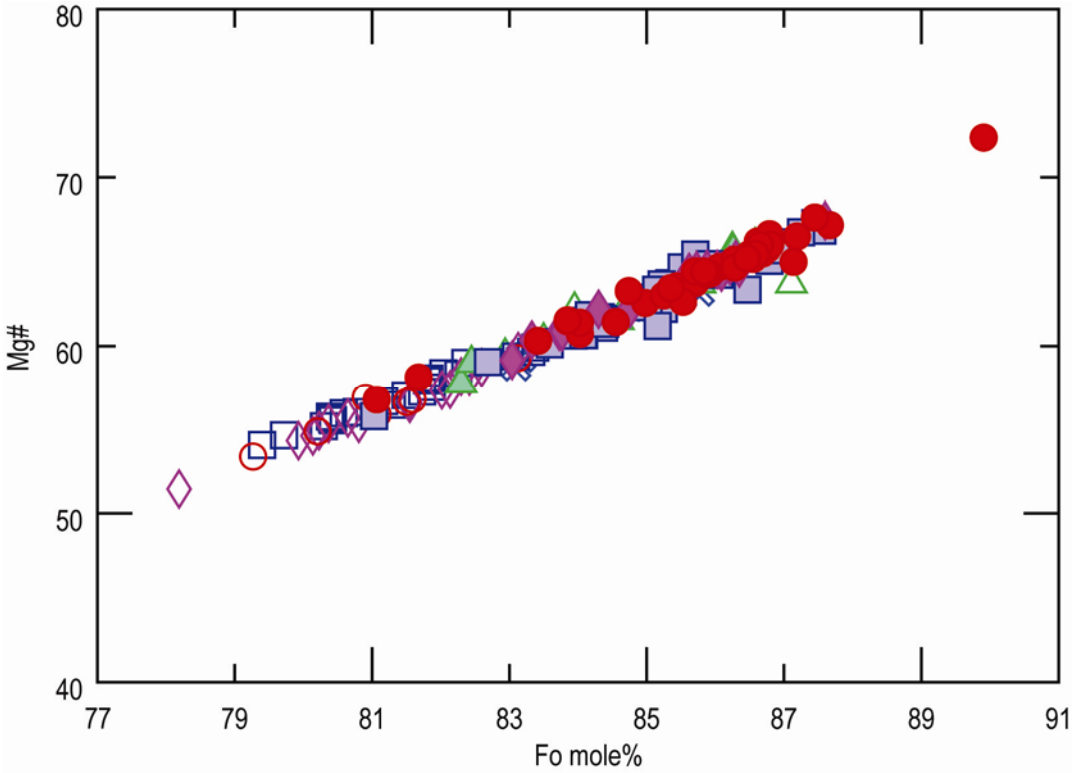


Fig. 13. Fo mole% vs. Mg# for glasses and bulk rock of this study. All values are calculated using petrolog software by Danyushevsky. Fo mole% for MI were obtain from EPMA analysis of the relative host. For open glass and bulk rock Fo mole% were obtained using the same software by calculating the composition of the olivine in equilibrium with the relative glass composition using Ford et al. (1983) equations. Mg# of MI are from corrected composition as described in the text. Mg# = 100*Mg/(Mg+$Fe^{2+}$). Symbols are as in figure 12.

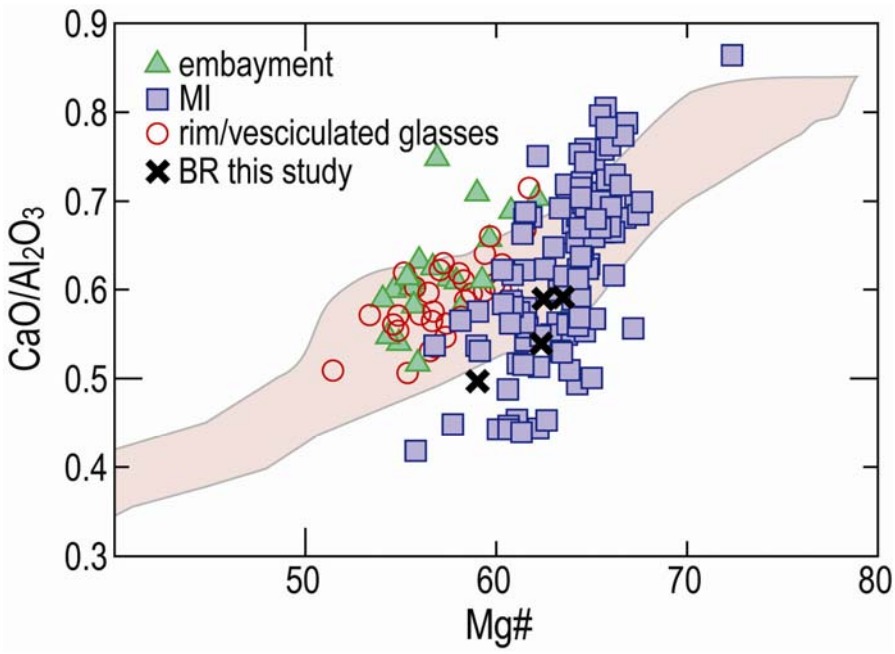


Fig.14. Mg# vs. $CaO/Al_2O_3$ diagram for corrected MI and open glass. The Pink background represents contents of bulk rocks from literature (Di Girolamo et al., 1984; D'Antonio et al. 1999; De Astis et al., 2004). It should be noted that the negative correlation is due to the crystallization of diopside along with olivine.

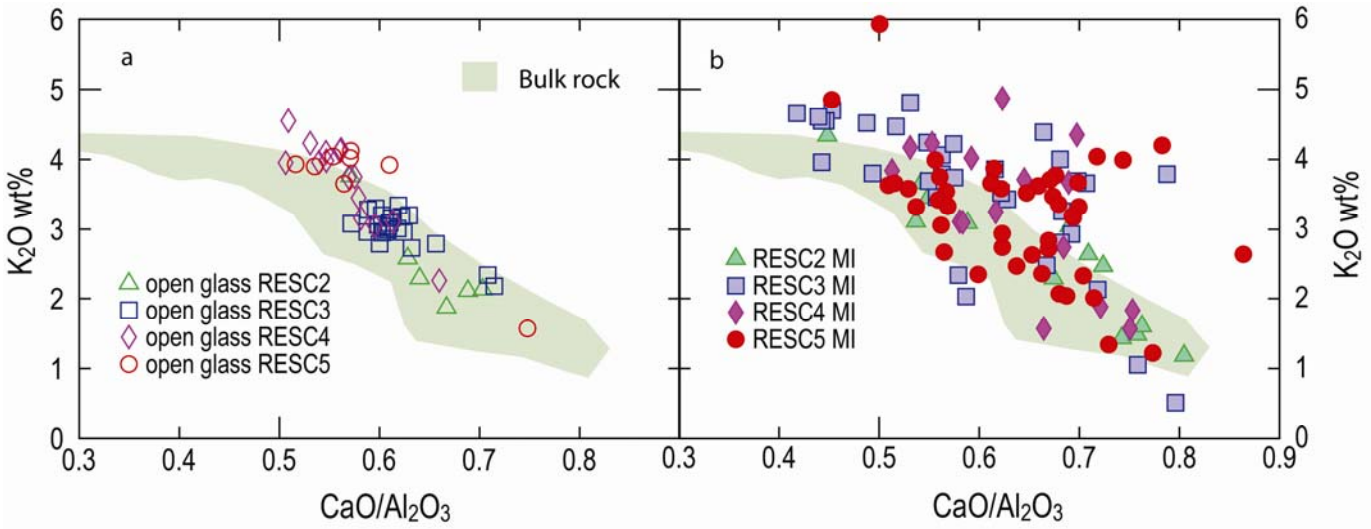


Fig. 15. $K_2O$ vs. $CaO/Al_2O_3$ for a) open glass composition and b) corrected MI, also showed are bulk rock compositions from literature (gray background). Note the MI wider spanning in respect to open glass. Symbols as in figure 12.

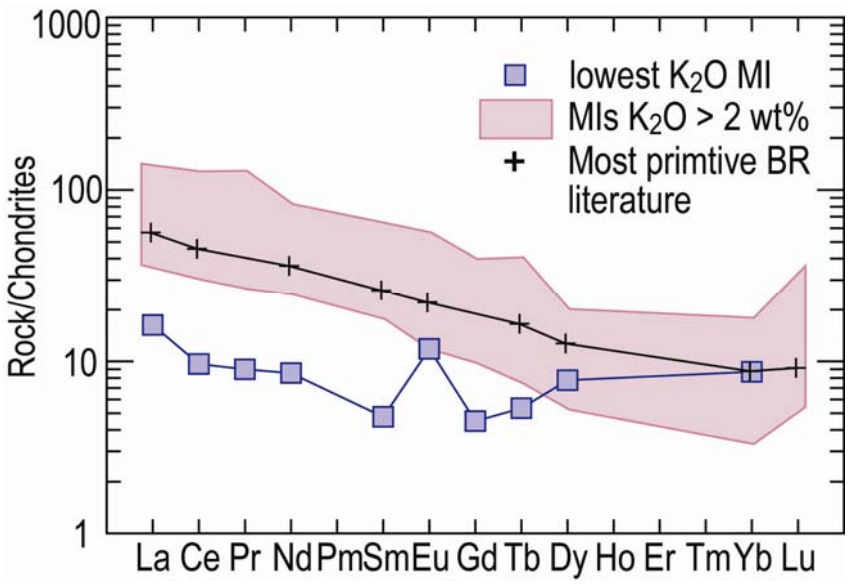


Fig. 16. REE distribution for corrected MI of the Solchiaro eruption. The lowest $K_2O$ MI (blue squares), $K_2O$-rich MI and the most primitive bulk rock of Solchiaro eruption (De Astis et al., 2004) are shown in the spider diagram from Nakamura (1974). Note the quasi-flat signature and the Eu positive anomaly of the lowest $K_2O$ MI.

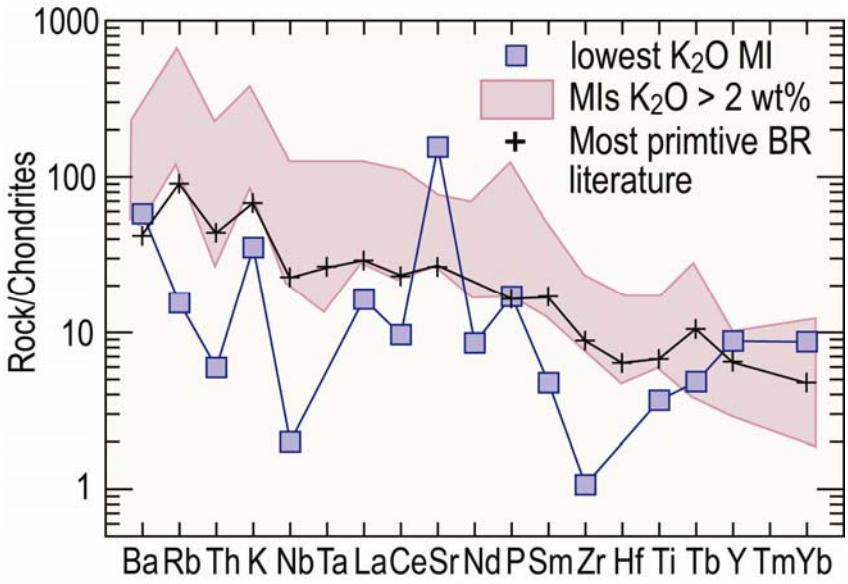


Fig. 17. Incompatible element distributions based on spider diagram from Thompson (1982). Note the high depletion of certain elements (Zr, Rb, Th, and Nb) for the lowest $K_2O$ MI and the strong positive Sr anomaly.

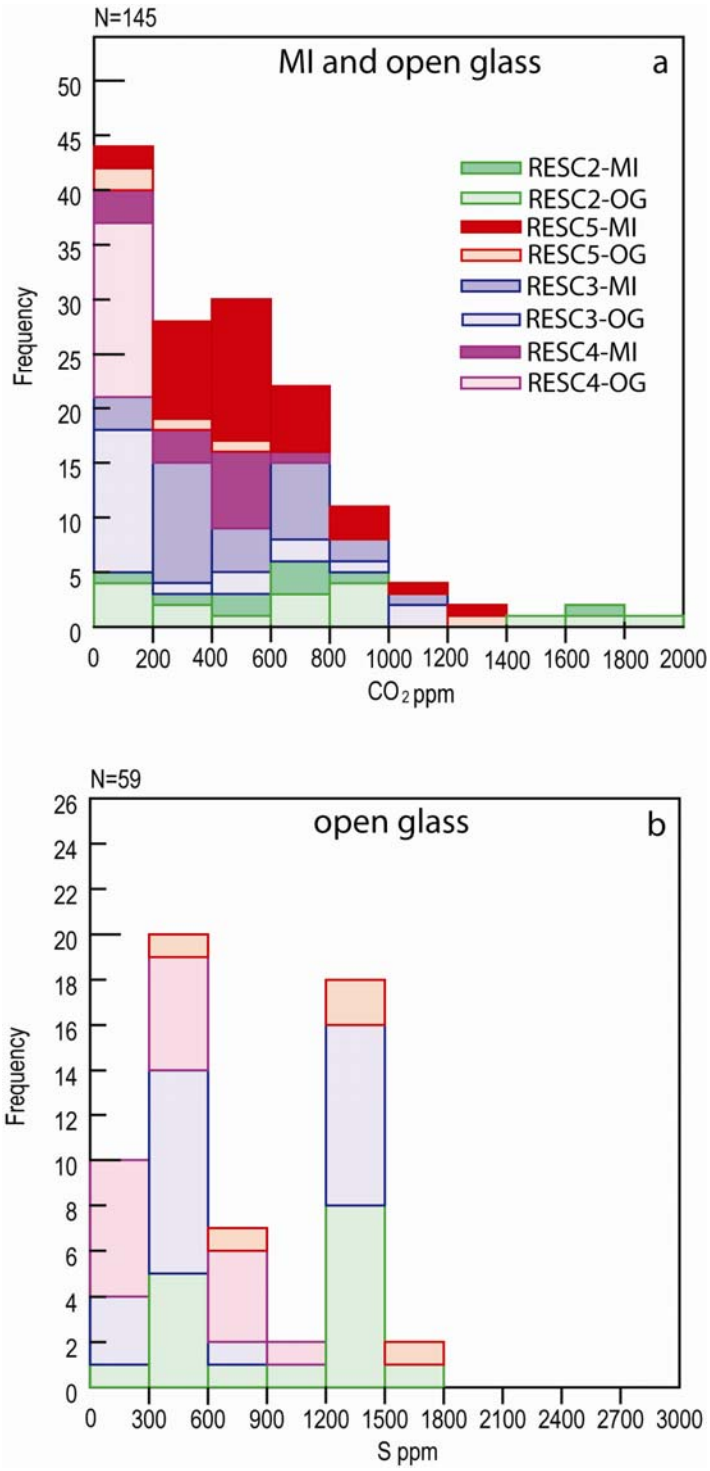


Fig 18. a) $CO_2$ contents of corrected MI and open glass from SIMS analysis. Note that glasses from sample RESC2 show the highest contents followed by RESC5, RESC3 and RESC4. b) histogram of S contents of open glass. Note that RESC2 and RESC5 show the highest contents. OG= open glass; N= number of observations.

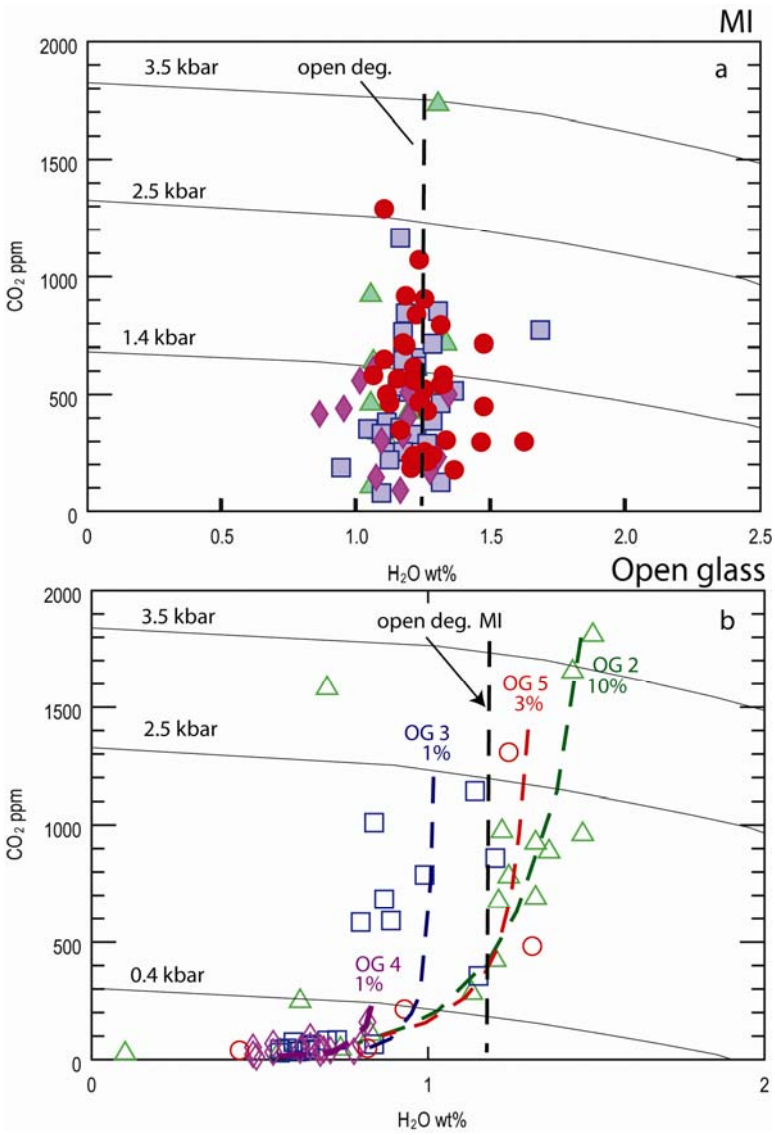


Fig. 19. $CO_2$ vs. $H_2O$ plot. Isobars (grey lines) are calculated using volatile.calc from Newman and Lowenstern (2002) considering $SiO_2$= 49 wt% and 1200 ºC. a) Degassing path of MI for all samples (black dashed line) is consider to be open system degassing. b) Degassing path (dashed colored line) are calculated using the same software assuming 1200 ºC and $SiO_2$= 49 wt%. Open glass of sample RESC2 (OG 2) is interpreted to represent closed system degassing (green dashed line) with 10% initial gas phase. Open glass of sample RESC5 (OG 5) is interpreted to represent closed system degassing (red dashed line) with 3% initial gas phase. Open glass of sample RESC3 (OG 3) is interpreted to represent closed system degassing (blue dashed line) with 1% initial gas phase. Open glass of sample RESC4 (OG 4) is interpreted to represent closed system degassing (purple dashed line) with 1% initial gas phase. Symbols are as in figure 12.

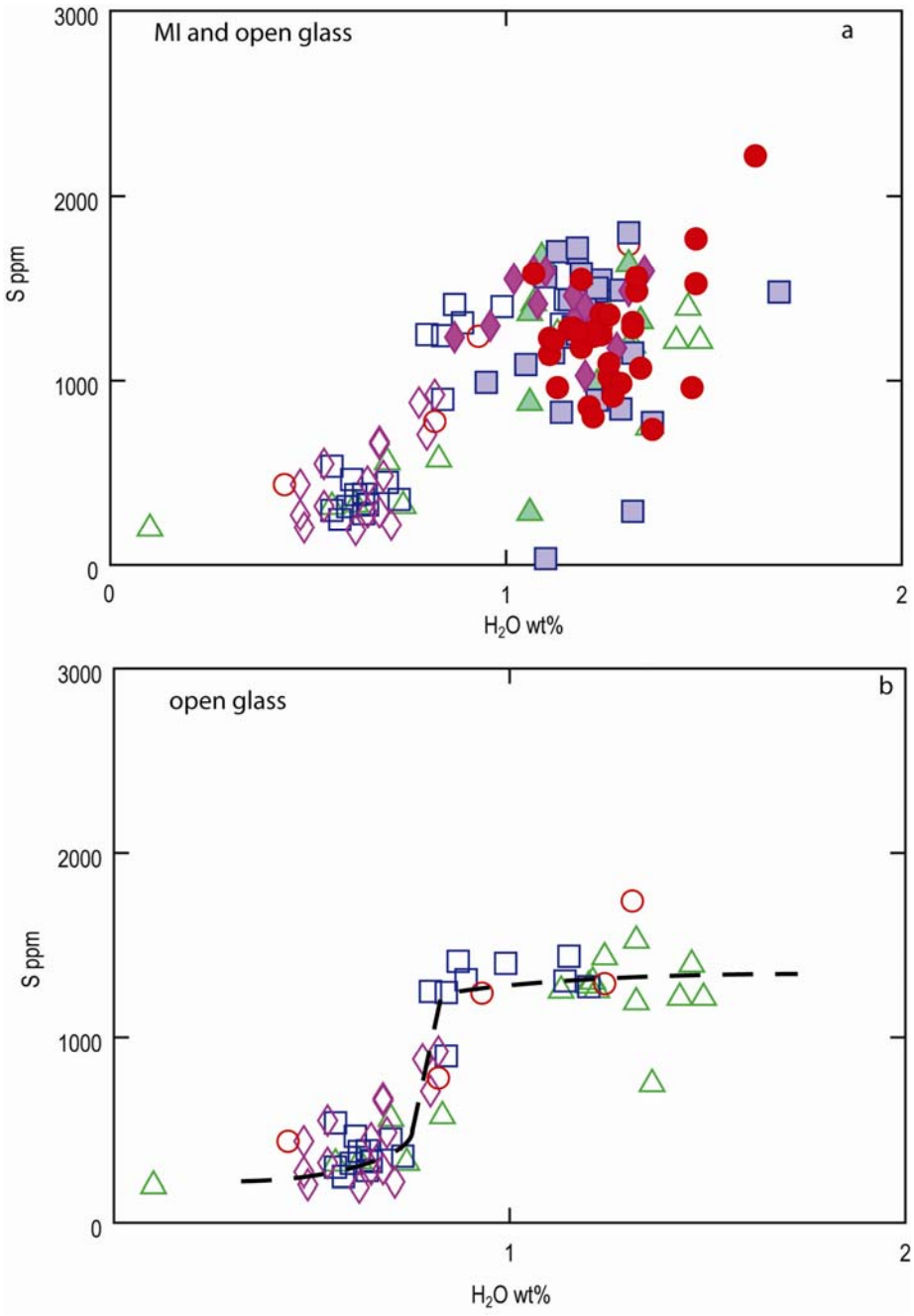


Fig. 20. $H_2O$-S systematic of glasses of this study. a) MI (filled symbols) and open glass (empty symbols) showing no correlation if considered as a whole. b) Open glass from all sample showing correlation interpreted as S-$H_2O$ degassing path (black dashed line).

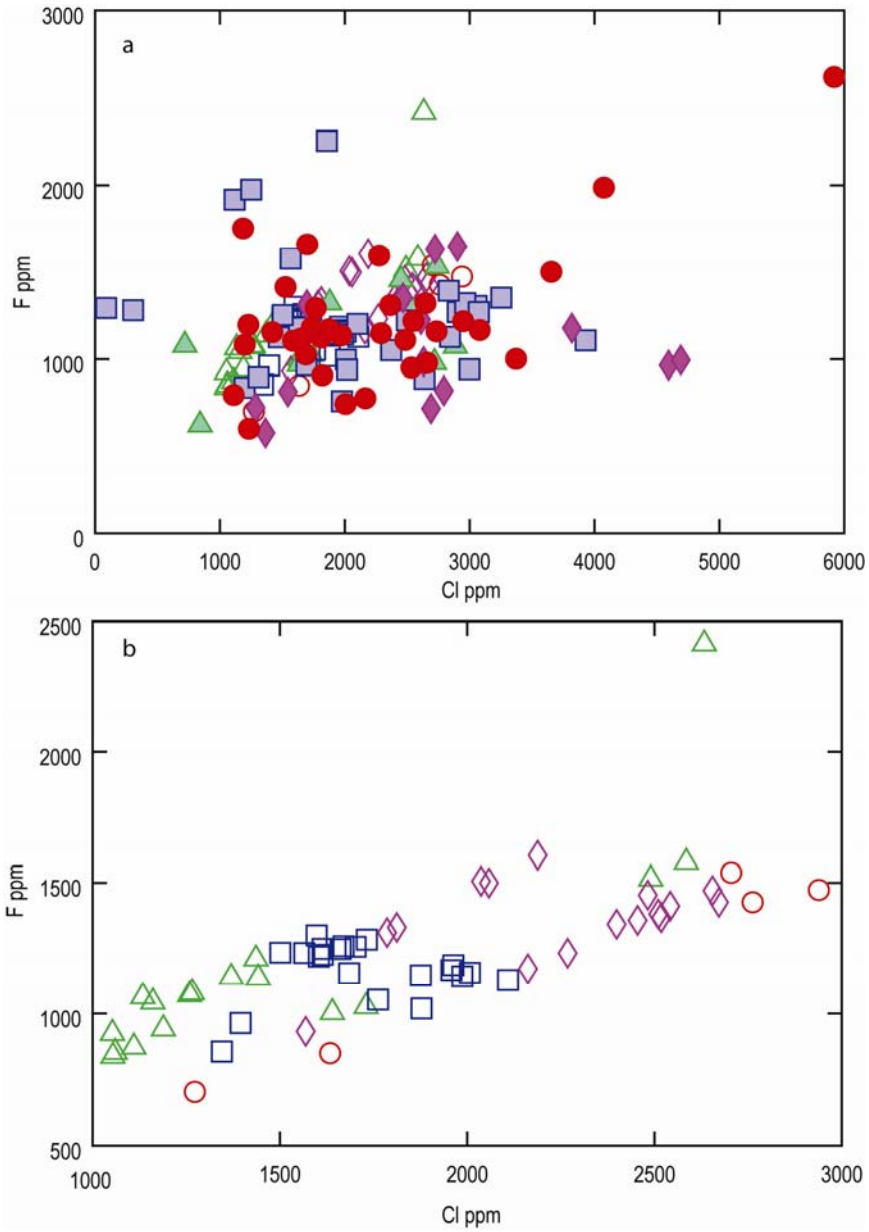


Fig. 21. Cl-F systematic of glasses of this study. a) MI (filled symbols) and open glass (empty symbols) showing no correlation if considered as a whole. b) Open glass from all sample showing correlation indicating F and Cl are retained in the melt as the system evolved (lowest content are mostly from sample RESC2).

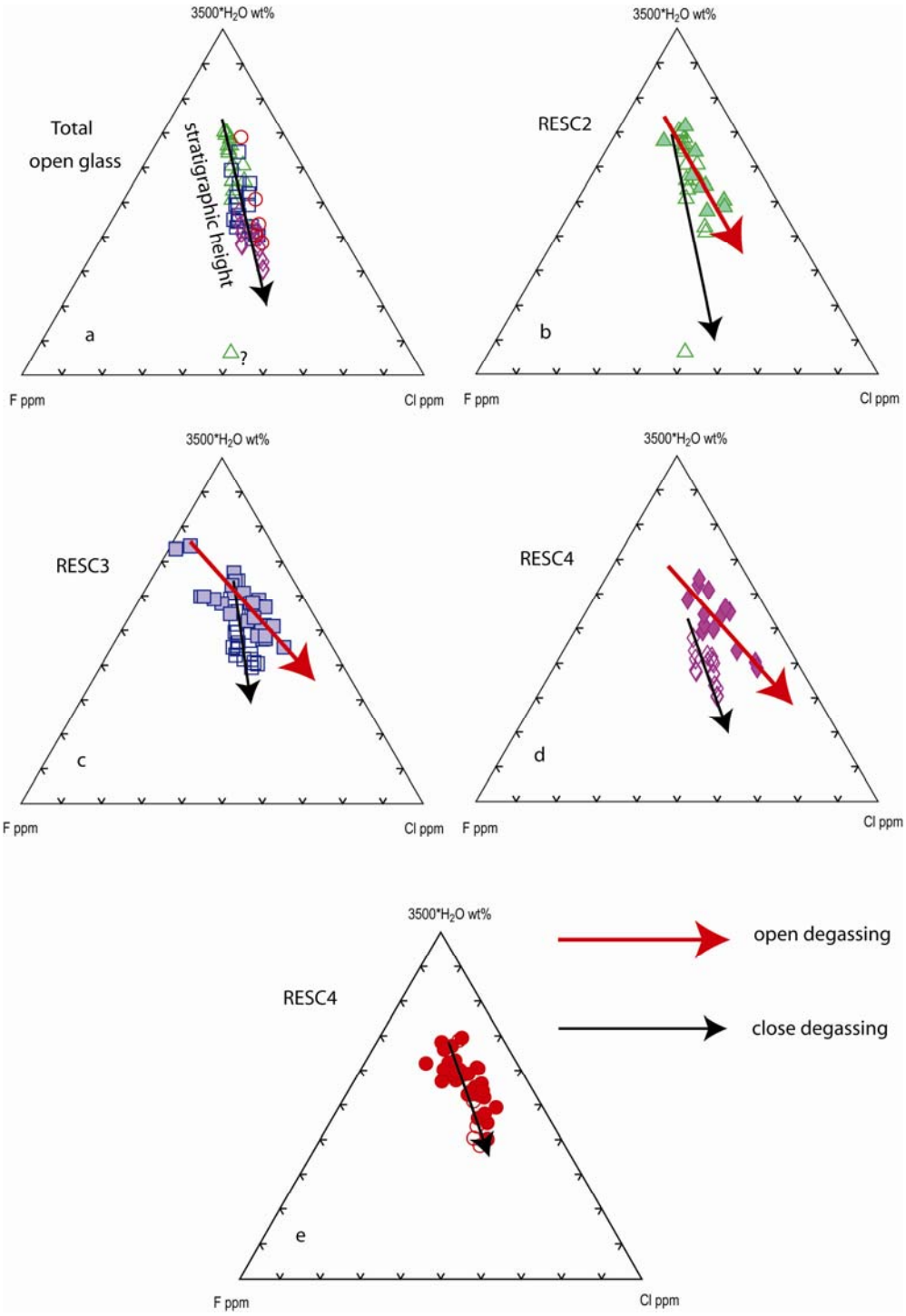


Fig. 22. F-$H_2O$-Cl triangular diagrams. a) total open glass showing a trend interpreted as a degassing of the Solchiaro eruption under open system conditions also suggested by $CO_2$-$H_2O$ systematic in figure 19. b) MI and open glass from sample RESC2 (bottom of the stratigraphic column) with MI showing slight different behavior relative to open glass. c) MI and open glass from sample RESC3 (6 m higher than RESC2 in the

stratigraphic column) with MI that show different behavior relative to open glass. d) MI and open glass from sample RESC4 (15 m higher than RESC3 in the stratigraphic column) with MI showing very different behavior relative to open glass. e) MI and open glass from sample RESC5 (close to the volcanic vent) with MI showing the same behavior relative to open glass. Note, especially in sample RESC3 and RESC4, the different trend between MI and open glass due to degassing at different condition (open for MI and closed for open glass).

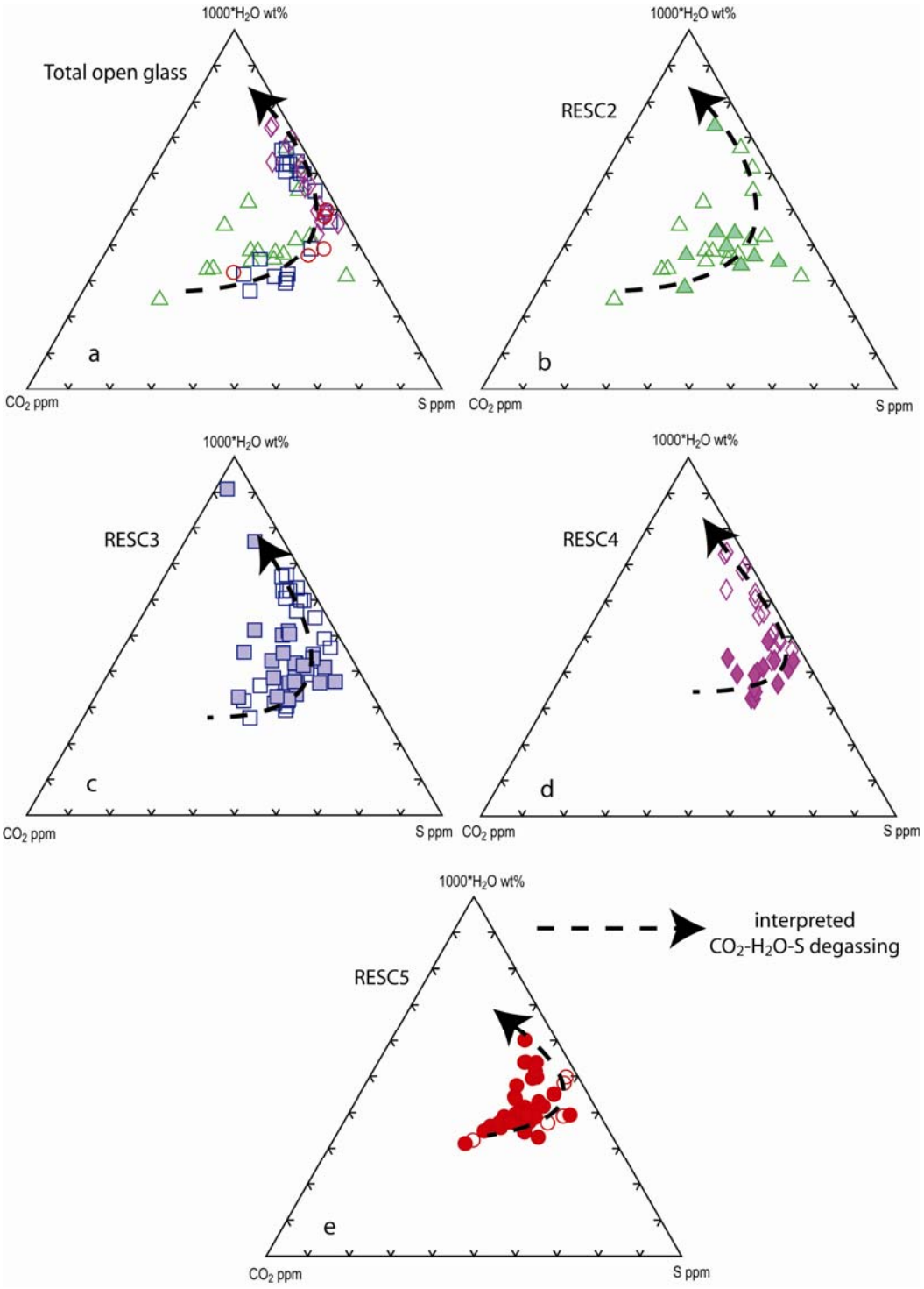


Fig. 23. CO-$H_2O$-S triangular diagrams. Black dashed arrows are interpreted degassing paths. Data indicate that the first volatile to dissolve is $CO_2$ but when it reach certain critical concentration also S start to exsolve from the melt and higher proportion of $H_2O$ is dissolved into the melt. Especially for sample RESC5, MI show a well defined trend. Symbols are as in figure 12.

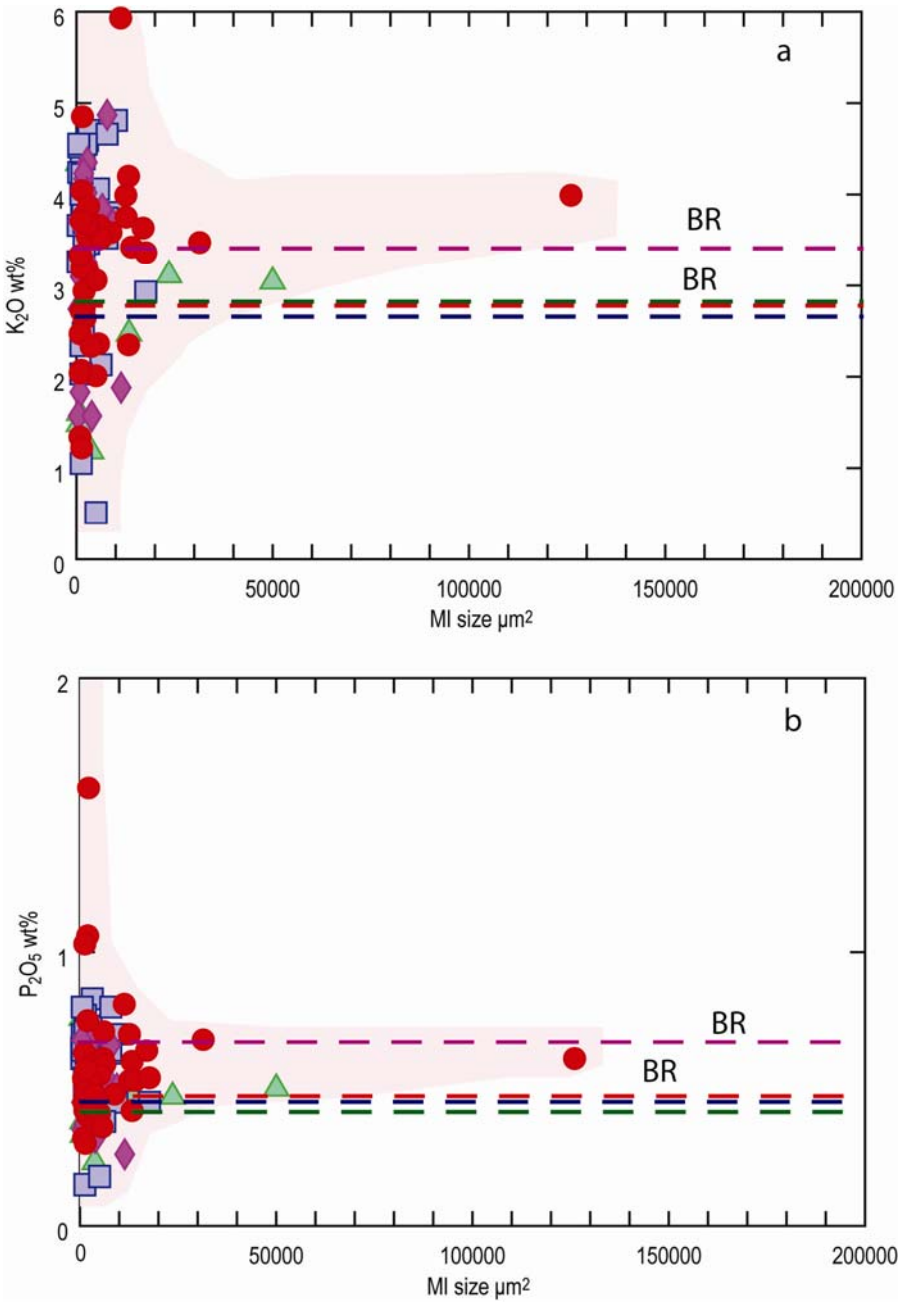


Fig. 24. MI size vs. $K_2O$ (a) and $P_2O_5$ (b) plots. Dashed lines represent the bulk rocks of each sample: green is RESC2, blue is RESC3, purple is RESC4 and red is RESC5. The pink area in the background is an interpreted field suggested by the data. Note that $K_2O$ and $P_2O_5$ approach the bulk rock contents increasing the size of MI. the size of MI was calculated as described in the text. Symbols are as in figure 12.

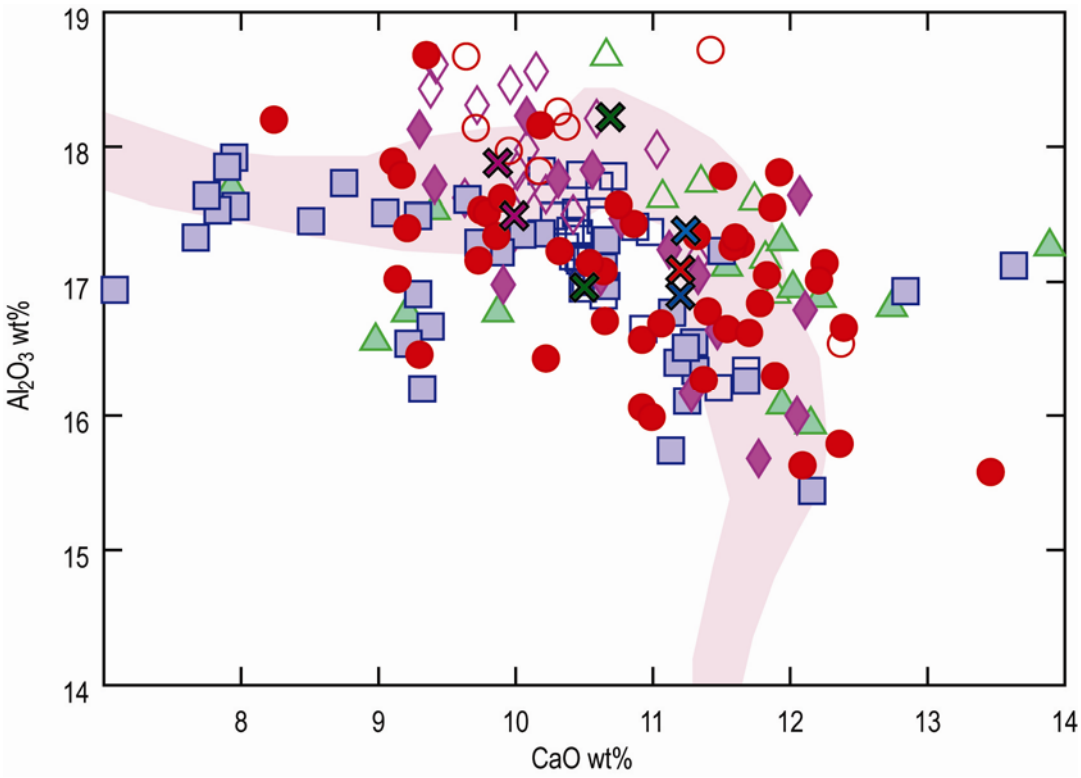


Fig. 25. Diagram showing the variation of CaO and $Al_2O_3$ in MI open glass and bulk rock from this study and from literature (pink background). Note that most of the MI composition overlap the bulk rock area. Symbols are as in figure 12.

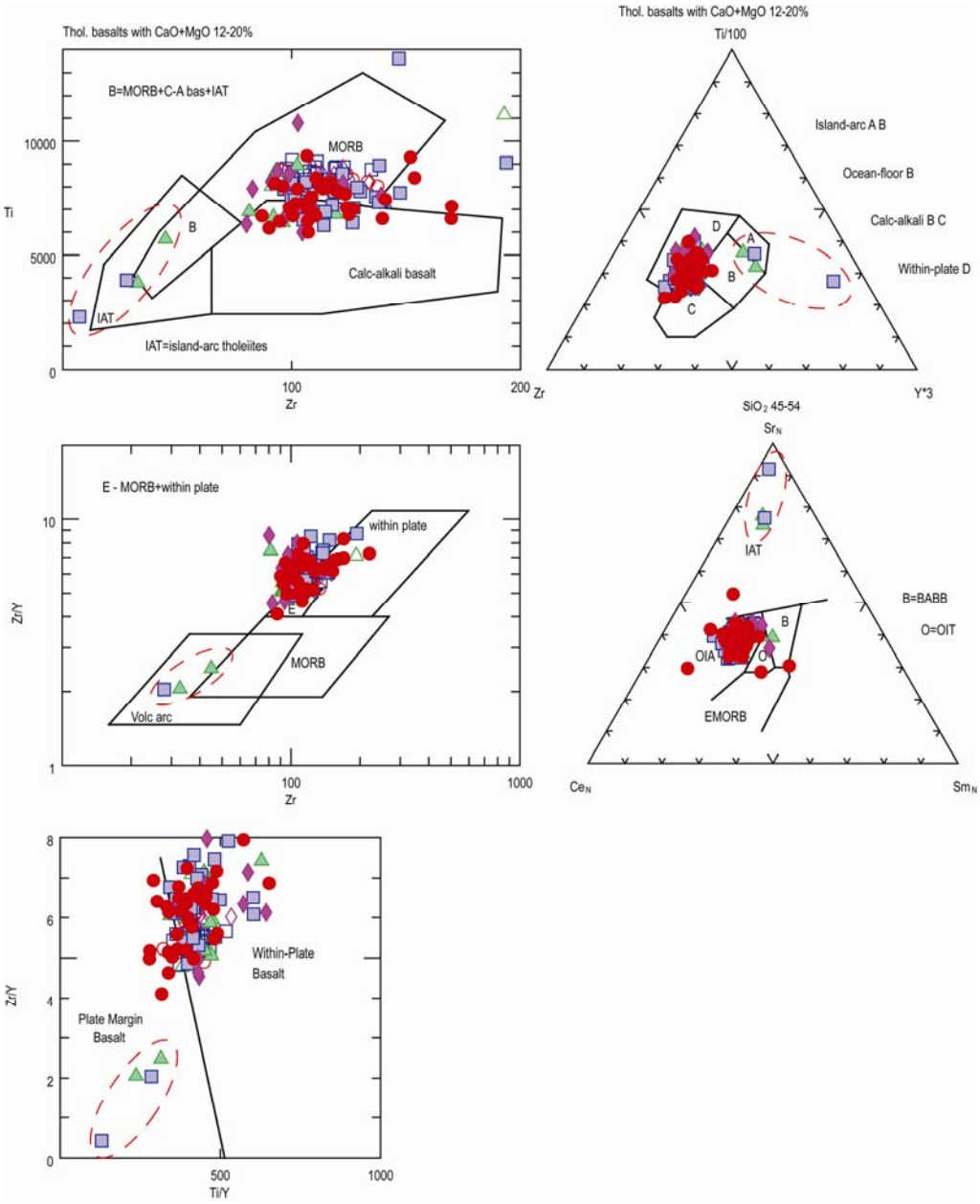


Fig. 26. Discrimination diagrams for basaltic rock showing 2 types of melt (dashed red ellipse) for the Solchiaro eruption based on MI. most of the MI compositions show affinity with within plate basalt. The 4 MI showing affinity with volcanic arc basalt are from the $K_2O$-poor MI group. Symbols are as in figure 12.

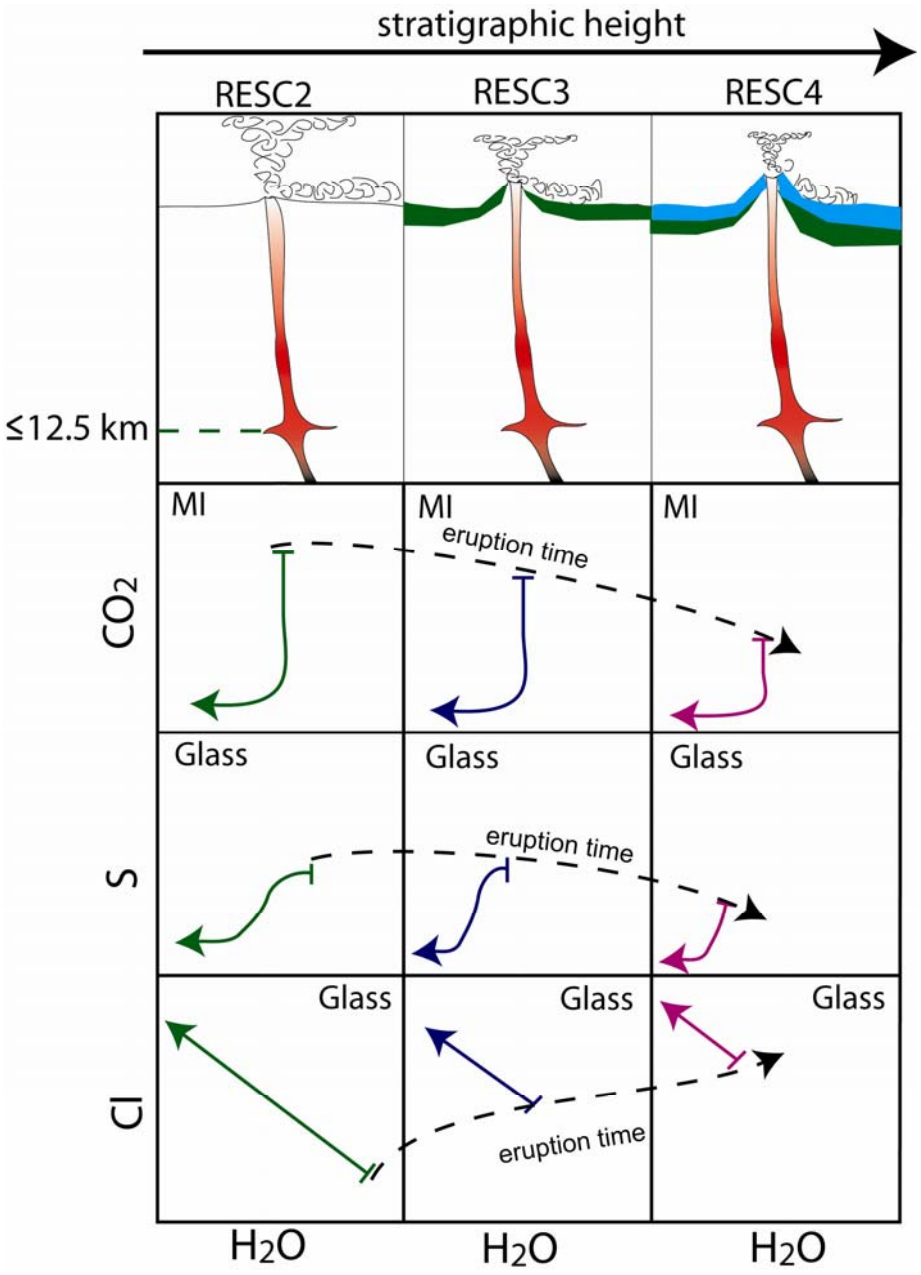


Fig. 27. Schematic evolution for volatiles of the Solchiaro eruption.The magmatic chamber is assumed to a minimum depth of 12.5 km (recorded by the highest pressure recorded in sample RESC2). The system degassed through time and $CO_2$-S dissolved into the melt decreased while F-Cl increased.